universität wien

DIPLOMARBEIT

Titel der Diplomarbeit

Start Configurations for Simulation of Ionic Liquids: Generation and Assessment

Verfasserin

Sonja Maurer

angestrebter akademischer Grad

Magistra der Naturwissenschaften (Mag. rer. nat.)

Wien, 2010

Studienkennzahl lt. Studienblatt:	A 419
Studienrichtung lt. Studienblatt:	Diplomstudium Chemie
Betreuer:	Prof. Othmar Steinhauser

Danksagung

Mein besonderer Dank gilt meinen Betreuern Prof. Othmar Steinhauser und Dr. Christian Schröder für ihre fachliche und kompetente Unterstützung.

Weiters möchte ich mich auch bei meinen Gruppenkollegen bedanken, die mir unermüdlich mit Rat und Tat zur Seite standen und mir mit ihrer lustigen Art und jeder Menge Schokoladenkekse den Arbeitsalltag versüßten.

Natürlich darf auch meine Familie und mein Freund nicht fehlen, die mich immer unterstützten und motivierten bei all meinen Vorhaben, und meine Freunde, auf die ich jederzeit zählen kann.

Zusammenfassung

Diese Arbeit hat zwei Schwerpunkte. Einerseits soll eine Methode gefunden werden, um schnell und einfach ein Startsystem für eine Simulation zu generieren. Andererseits soll das so erzeugte System geeignet sein für eine anschließende Simulation mit einer kurzen Equilibrierungsphase von nur 1.5 Nanosekunden.

Nach Abschluss der Equilibrierung soll das System im Gleichgewicht sein. Als Modell-System diente eine ionische Flüssigkeit bestehend aus dem Kation 1-Butyl-3-methyl-imidazolium und dem Anion Triflat. Es wurden zwei Methoden für die Herstellung von Startkonfigurationen miteinander verglichen und das Programmpaket PACKMOL wurde zur Methode der Wahl. Es wurden verschiedene Ansätze versucht um die Konfigurationen in das Gleichgewicht zu bringen, wie z.B. Ladungsskalierungen. Die Beurteilung, ob sich das System nun im Gleichgewicht befindet, wurde anhand von Korrelationsfunktionen getroffen. Dabei wurde das rotationale Moment $\mathbf{M}_D$ mit sich selbst korreliert. Später wurde noch ein weiteres Modell-System hinzugefügt, bestehend aus dem Kation 1-Ethyl-3-methyl-imidazolium und dem Anion Triflat. Durch die Hinzunahme konnte eine Abhängigkeit der Relaxation vom Startwert einer Korrelationsfunktion erkannt werden.

Abstract

This thesis has two main points. On the one hand, a method should be found to generate starting structures for simulations in a fast and easy way. On the other hand, should this newly created structure be adequate for a simulation with just a short phase of equilibration of 1.5 nanoseconds.

The system should be in equilibrium at the end of the equilibration. As a model system a ionic liquid, consisting of the cation 1-Butyl-3-methyl-imidazolium and the anion Triflate, was chosen. Two methods for the generation of start configurations were compared and PACKMOL became the method of choice. Different approaches were tried to equilibrate the starting structures, such as the scaling of the charges. The assessment, if a system is in equilibrium or not, was done via correlation functions. For that matter, the rotational moment $\mathbf{M}_D$ was correlated with itself. Later, another model system was added, consisting of the cation 1-Ethyl-3-methyl-imidazolium and the anion Triflate. In doing so, a dependency of the relaxation to the start configuration of a correlation function could be identified.

Contents

1 Introduction

1.1 Ionic Liquids

Ionic Liquids (IL), also known as liquid electrolytes, ionic melts, ionic fluids, liquid salts, fused salts or ionic glasses, have become quite popular recently. ILs are salts where at least one component is an organic compound and they consist just of ions. Where substituted pyridiniums and imidazoliums provide the cation most of the time, there can be found organic and inorganic compounds as anions [1–3], such as halides, borates, phosphates, sulfonates and triflates.
ILs are liquid below 100°C. A sub-group of ILs are the so-called Room-Temperature Ionic Liquids (RTIL); they are actually liquid at or below room- temperature.
Although they are known since the beginning of the 20^{th} century their physical properties made them interesting to the industry just in the last 30 years. It was then, when the green chemistry movement started looking for alternatives for the most damaging solvents such as benzene. The goal of this movement is to reduce or even better eliminate the use of hazardous substances and ILs provided them with a number of interesting properties. ILs do not evaporate due to their low vapour pressure [4], they are non-volatile, but good solvents for quite a lot of inorganic and organic materials, they are immiscible with several organic solvents and therefore provide a non-aqueous polar alternative [5–7] for two phase systems, they cover a wide temperature range [8] and they can be made moisture and air stable. Because those volatile solvents are used in great quantities and are difficult to contain, ILs are said to have a low impact on the environment and human health.
In this manner ILs have found their way into industrial applications as catalysts [9–11], solvents, paint additives and many more. The spectrum of applications is growing steadily.

1.2 Simulation of Ionic Liquids

The industry is constantly looking for new, task specific ILs [12]. Considered that the summation of all possible combinations of cations and anions results in about 10^{12} ILs, one is keen to avoid

to test each for its physical and chemical properties. Therefore a further understanding of the basic interactions of ILs and their solvent characteristics are vital.
At that point the computational investigation comes into operation. By simulating ILs, instead of investigating them by experiment, it is possible to gain more detailed information. Therefore, you have to collect molecular dynamics simulation data, i.e. trajectories. This trajectories can be used e.g. for the generation of a dielectric spectrum, which can be again compared to the one from the experiment. By comparing the results with those of the experiment one is able to improve the force field used for the simulation.
But, it makes only sense to collect that data, when the system is in equilibrium. Therefore, it is vital, that the system is well mixed and that there are no other 'artefacts' of the construction of the system, like a crystal structure. Due to the fact, that ILs are charged molecules, they are able to order themselves in a way other molecules do not. This is also known as 'charge ordering'. This effect is quite strong and will last through the equilibration phase and the following simulation. To gain as fast as possible the relevant data, the time needed for equilibration should be short.
In this thesis I concentrate on two main points. First, the construction of systems containing Ionic Liquids and second, the assessment of these newly created structures.
In the Methods section I will discuss the two different programs, which can be used for creation of starting configurations. In the Theory section I will give an overview about the theoretical background needed for the assessment of the structures. In the following chapters I will give the results of my work and a discussion.

2 Methods

2.1 Lattice

Lattice is a Fortran90 program and was written by Dr. Christian Schröder, a group member. It is designed for packing cations and anions into a cubic box.

2.1.1 Mode of Operation

The program requires certain information to be able to serve its purpose. This information will be given via an input file (see Fig. 2.1).
This file contains the crd-files - coordinate files - of the cation and anion, the number of ion pairs and the box length of the cube, in which the ions will be packed. Furthermore it includes a maximum allowable energy.
After reading the input file, the program multiplies the number of ion pairs *ip* by 2 to get the total number of molecules m. Then it will test which number n to the third-power n^3 will be greater than or equal to m. After this, the given box length will be divided by n to allocate the edge length of a rectangular cuboid in which one ion will be packed. That way the program assigns a certain volume, which is the same for the cation and the anion.
Now the program is able to start filling the box. Starting point is one corner and from there on the ions will be placed alternating in all three dimensions, first the x-dimension, second the

```
CRD1 bmim.crd
CRD2 trif.crd
CRD3 output_name.crd

BOXL 69.
NPAIR 891
NSTEP 1000
NSAVE 200
NPRINT 100
ULIMIT 2000
```

Figure 2.1: A model input file for lattice. The maximum allowable energy is given by ULIMIT.

y-dimension and then the z-dimension. It is possible that not all z-layers are filled. Then the z-direction has to be scaled in order to obtain a cube. This is done by dividing the z-direction by the number of occupied z-layers. Nevertheless, it is still possible that the last layer includes a hole because there aren't any ions left to fill it. This is due to the difference between n^3 and m.

This process will be illustrated by an example:

15 ion pairs are to be packed in a box with the edge length of 10Å. The total number of molecules is

$$m = ip \cdot 2 = 30. \tag{2.1}$$

The next step is to allocate n, which is 4, because:

$$n^3 = 64 \geq 30 \tag{2.2}$$

n cannot be 3, because $3^3 = 27$, which is less than $m = 30$. Since $n = 4$, the box length will be divided by it

$$10/4 = 2.5, \tag{2.3}$$

which results in an edge length of 2.5Å for the cuboid for 1 ion. The packing is started at $(x, y, z) = (0, 0, 0)$ and 16 ions will be placed in the first layer. The other 14 ions will be placed in the second layer but two places have already to be left free, this is the same for the last two layers (Fig. 2.2). This two layers are used to rescale the z-direction in order to obtain a cube (Fig. 2.3). The new edge length in z-direction measures 5Å.

After packing the molecules into the box, the time consuming part starts. The problem is that the anticipated space for an ion is not big enough and therefore parts of molecules will overlap.

To get rid of these clashes the program calculates a Lennard-Jones like energy U of each residue i, according to this formula:

$$U_i = \sum_a \sum_j \sum_b \frac{4000}{r^{12}_{ia,jb}}, \tag{2.4}$$

where a is each atom of the residue i and b is each atom of the neighbours j.

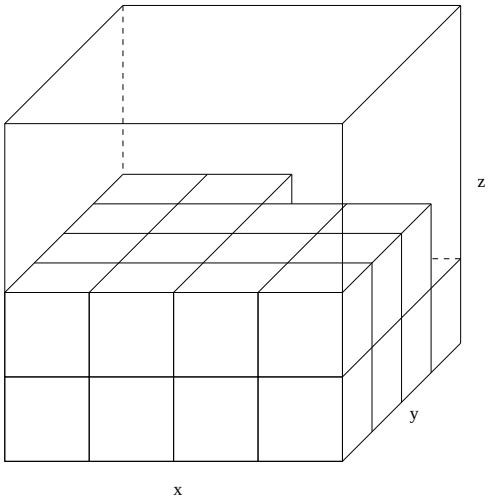

Figure 2.2: The box would look like this without the scaling of the z-direction. Only the first layer is filled entirely with molecules. In the second layer there are already two places left free.

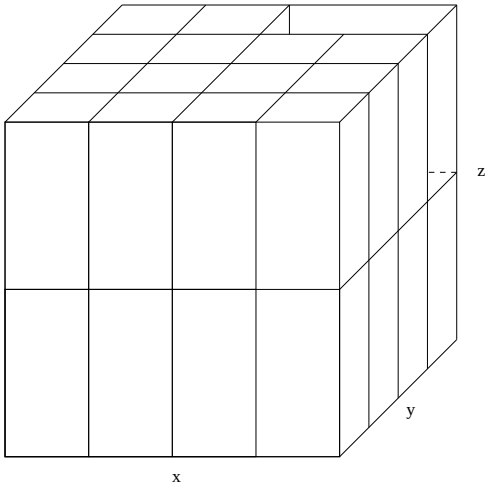

Figure 2.3: This is the box after the rescaling of the z-direction. There are still two places left free, due to the fact, that there are no molecules left, which can be packed into it. This hole has to be get rid of by the use of simulation.

Now, the residue with the highest U_i is identified. Then, all the distances from each atom of this ion are measured to the atoms of each other ion of all the 26 neighbouring boxes. The smallest distance $r_{a,b}$ is determined and it will be elongated by translation. Afterwards, the energy is updated. Now, the molecule will be rotated in the three-dimensional space by three random Eulerian angles. The next step is to test, if the new configuration has a better energy than the old one. If it is better, it will be saved, otherwise the old configuration, before the rotation, is restored. Then, the next residue with the highest U_i is identified. The program loops over all ions until the energy is smaller than the given maximum energy.

This program has some disadvantages which makes it uninteresting for further use. First, the last layer in z-direction contains a whole most of the time and one has to get rid of it during simulation. Second, the alternating filling results in a crystal structure which has to be melted during simulation and this is a tedious process. Third, the time required for getting an output ranges between minutes and hours, this is worse in comparison with PACKMOL.

2.2 PACKMOL

PACKMOL is a software package for building initial configurations which can be used in molecular dynamics simulations. The software was developed by L. Martínes [13] and others in Brazil and can be downloaded for free from the website http://www.ime.unicamp.br/∼martinez/packmol.

The program is able to pack millions of atoms, which can belong to different types of molecules, into a box of defined size. Furthermore it is able to pack a selection of molecules - or even atoms of a molecule - into regions within that box. In this manner, the program can build complex mixtures, solvate biomolecules in water or can construct even more ordered structures such as interfaces, lipid double-layers and micelles.
When molecules are assigned to a box, it is vital that molecules do not overlap each other. They must satisfy certain spatial arrangements. PACKMOL handles the distribution of molecules in a box as a packing problem. Therefore, atoms of different molecules have to keep a certain distance to each other. The time needed for a packing process ranges from a few seconds up to minutes. In order to get the program started the user has to provide an input file (see Fig. 2.4). The file contains the structure of each type of molecule and the constraint, which the molecule has to satisfy. The structure can be read in as a PDB, Tinker, Moldy or Molden coordinate file.

```
tolerance 2.0
output seed_1.pdb
filetype pdb
seed 243

structure bmim.pdb
number 891
inside cube 0. 0. 0. 69.0
end structure

structure trif.pdb
number 891
inside cube 0. 0. 0. 69.0
end structure
```

Figure 2.4: A model input file for PACKMOL. The structure of a molecule is given in pdb format.

2.2.1 Theoretical Background

By the use of the input file the program knows the coordinates of the atoms of each molecule. The origin of a molecule is its barycentre, the arithmetic average of the coordinates of the atoms, i.e. the centre of geometry. Thus, the coordinates of a molecule i with its atoms a can be written as

$$\mathbf{r}^{i,a} = (r_1^{i,a}, r_2^{i,a}, r_3^{i,a}). \tag{2.5}$$

A molecule can be moved by rotation and translation. Rotation takes place when a molecule is rotated around the axes x_1, x_2 and x_3 by the angles $\Theta^i = (\Theta_1^i, \Theta_2^i, \Theta_3^i)$. This is done via a

rotation matrix $R(\Theta^i)$:

$$R(\Theta^i) = \begin{pmatrix} c_1^i c_2^i c_3^i - s_1^i s_3^i & s_1^i c_2^i c_3^i + c_1^i s_3^i & -s_2^i c_3^i \\ -c_1^i c_2^i s_3^i - s_1^i c_3^i & -s_1^i c_2^i s_3^i + c_1^i c_3^i & -s_2^i s_3^i \\ c_1^i s_2^i & s_1^i s_2^i & c_2^i \end{pmatrix}, \tag{2.6}$$

where $s_k^i = sin\Theta_k^i$ and $c_k^i = cos\Theta_k^i$, for $k = 1, 2, 3$. For the translation the barycentre b will be relocated to $\mathbf{t}^i = (t_1^i, t_2^i, t_3^i)$. In that manner the coordinates of a molecule will be changed from $\mathbf{r}^{i,a}$ to the new position $\mathbf{r'}^{i,a}$ by a combination of the translation and rotation:

$$\mathbf{r'}^{i,a} = \mathbf{t}^i + R(\Theta^i) \cdot (\mathbf{r}^{i,a} - b) + b \tag{2.7}$$

As a next step the program has to perform two tasks. First, it has to find the specific translation and rotation to be able to match the given constraints and second, the atoms of two molecules *i*, *i'* have to have a minimum-distance from each other, which should not be less than d_{tol}, a specified tolerance given by the user,

$$|| \mathbf{r}^{i,a} - \mathbf{r}^{i',a'} || \geq d_{tol}. \tag{2.8}$$

If $c^{i,a}$ is the number of constraints which belong to the atom a of the molecule *i*, then the number of constraints can be written as

$$g_l^{i,a}(\mathbf{r}^{i,a}) \leq 0, l = 1, \ldots, c^{i,a}, \tag{2.9}$$

where $g_l^{i,a}$ is the geometrical constraint. Equation 2.9 will be positive, if the constraint is not fulfilled and negative otherwise. Equation 2.8 and 2.9 are so called objectives and can be put together to form the function $f(t, \Theta)$:

$$f(t,\Theta) = \sum_{i=1}^{N}\sum_{a=1}^{n_i}\left(\sum_{i'=i+1}^{N}\sum_{a'=1}^{n_{i'}} max\{0, d_{tol}^2 - || \mathbf{r}^{i,a} - \mathbf{r}^{i',a'} ||^2\}^2\right) \tag{2.10}$$

$$+ \sum_{i=1}^{N}\sum_{a=1}^{n_i}\left(\sum_{i=1}^{c^{i,a}} max\{0, g_l^{i,a}(\mathbf{r}^{i,a})\}^2\right), \tag{2.11}$$

where N is the total number of molecules, n_i is the number of atoms of the molecule i and $n_{i'}$ is the number of atoms of the molecule i'. $f(t, \Theta)$ is zero, when both objectives are fulfilled otherwise it will be positive.

Now the function $f(t, \Theta)$ can be minimized. Since $f(t, \Theta)$ is continuous, it can be differentiated to first order and the global solution is reached when $f(t, \Theta) = 0$.

Respective to the computational cost the second term of $f(t, \Theta)$ scales linear in time whereas the first term increases by square with the number of atoms. This gets quite cumbersome for larger systems.

Thus, PACKMOL uses the so-called Linked Cell technique. For that matter the box is intersected into smaller bins with the edge length of d_{tol}. Each atom is now assigned to a bin and only interactions of atoms in the same bin or between neighbouring bins have to be computed. Using this technique the scaling can be reduced and it scales linear with the total number of atoms.

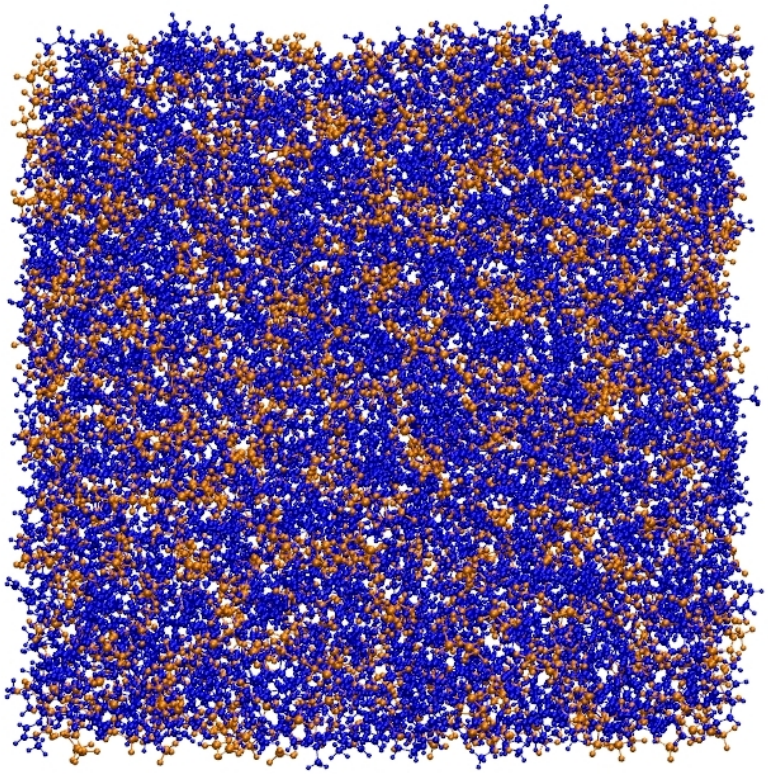

Figure 2.5: A box with 69Å edge length packed by PACKMOL. The cations (1-Butyl-3-methyl-imidazolium) are coloured in blue and the anions (Triflate) are orange.

For optimizing the minimization process PACKMOL uses an iterative method called GENCAN. GENCAN uses the Newtonian method for going into the minimum using the gradient.

The program package PACKMOL provides a user friendly interface and convinces with its short computation time. Furthermore, the built boxes are well mixed (see Fig. 2.5). The only two disadvantages are, that the output-file has to be converted from a pdb- into a crd-file, in order to use it with the molecular dynamics program CHARMM, and furthermore the coordinate system of the converted file has to be adjusted by half of the box length. This is due to the fact, that

PACKMOL has its origin at the point $(x, y, z) = (0, 0, 0)$. In CHARMM the coordinate system starts at minus the half of the boxlength and goes to plus of the half. Therefore, one has to shift the whole origin by half of the box length.

2.3 Simulation

CHARMM [14] (Chemistry at Harvard Molecular Mechanics) was the molecular dynamics program of choice. It was used for the minimization of the energy, the adjustment of the box length and the generation of trajectories.

2.3.1 Minimization

Each configuration, generated by PACKMOL, had a far too high energy. Thus, a minimization of the energy was necessary. CHARMM provides the user with a couple of minimization algorithms [15] to choose from. However, all methods calculate the derivative of the potential energy and some of them compute the second derivative too. With this information the program is able to adjust the coordinates in a way that the new conformation has a lower energy.
The simplest minimization method is the steepest descent algorithm. It is the method of choice to minimize unequilibrated conformations in a short time. Although it does not converge very well, the minimization is in general sufficient enough.
The coordinates are adjusted alongside the negative gradient at each step. The step size is the only adjustable parameter. It gets greater while the energy drops and the minimum approaches. Is there a rise in the energy, the miminum was missed and the step size is reduced.
All other methods converge better than the steepest descent algorithm, but the computation time increases significantly. Since reasonable values were reached with steepest descent, this method was used.

2.3.2 Adjustment of the Box Length

Some configurations were packed in larger boxes, than necessary. An adjustment of the box length was essential. Therefore, constant pressure and constant temperature dynamics [16] was done and the user has two methods to choose from, the weak coupling method for temperature and pressure control, which was the first being implemented, and a method for extended systems. In this thesis the extended version [16] of the algorithm was used. Here, the Hoover temperature control [17] finds its application. Simulation was carried out for ten-thousand steps this is the equivalent to ten picoseconds. For the piston-mass 500 amu were chosen and for the thermal

piston 500 $kcal \cdot ps^2/mol$. The updated box length was printed out for evaluation and used for the next dynamics, in case that it was necessary.

2.3.3 SCALAR-Command

The SCALAR-command [18] is a command to manipulate any scalar atom property. A diverse range of mathematical operations are at hand for manipulation, such as multiplication, addition and division but there are other operations, not mathematical ones, too. It can be used on all atoms or just a set of them.
In this thesis, the SCALAR-command was applied on some systems to reduce the charge of the whole set of atoms. When the command was used during the adjustment of the box length, the charge was reduced to just 10% of the original values. During the resizing process the charges were rescaled in steps of 10% to the original values.

2.3.4 Equilibration

After the minimization and maybe an adjustment of the box length, the actual simulation was carried out. The beginning of a simulation is also called the equilibration. It is very important to equilibrate a system, because this is the time when the kinetic and potential energy disperses itself through the system. It makes only sense to produce trajectories for analysis when a system is equilibrated. Naturally, one wishes that the time for equilibration is as short as possible.
Each system was equilibrated for 1.5 nanoseconds. This was done by constant temperature dynamics. Again the Hoover temperature control [17] was used with a piston mass of 500 $kcal \cdot ps^2/mol$ as already used in constant pressure dynamics. During the simulation trajectories were generated. The trajectories were needed for the calculation of the correlation functions. Besides, coordinate files were printed out every fifty picoseconds. These files were required for the calculation of the instantanious values of the rotational moment $\mathbf{M}_D$.

3 Theory

3.1 $\mathsf{M}_D, \mathsf{M}_J, \mathsf{M}_{tot}$

3.1.1 Total Collective Dipole Moment M_{tot}

The motion of molecules during a simulation can be described by their translation and rotation in space and, in addition, the molecule itself has the potential to move internally. The total collective dipole moment $\mathbf{M}_{tot}$ [19] is a parameter for describing an entire sample of molecules. Since the net charge of the system totals zero, $\mathbf{M}_{tot}$ is unique. If the calculated system is in equilibrium, the average of $\mathbf{M}_{tot}$ will be zero. Therefore it can be used to assess the quality of statistics of a simulation.

$\mathbf{M}_{tot}$ of the complete sample is calculated by multiplying the coordinates of an atom by its charge and the following summation over all atoms a and molecules i,

$$\mathbf{M}_{tot} = \sum_i \sum_a q_{i,a} \cdot \mathbf{r}_{i,a}. \tag{3.1}$$

Since the summation is done over all molecules, $\mathbf{M}_{tot}$ is a collective property.

$\mathbf{M}_{tot}$ can be expanded by dividing the inner sum by q_i, i.e. the net charge of a molecule, and multiplying the outer sum by the same factor,

$$\mathbf{M}_{tot} = \sum_i q_i \left(\sum_a \frac{q_{i,a} \cdot \mathbf{r}_{i,a}}{q_i} \right). \tag{3.2}$$

Now, $\mathbf{M}_{tot}$ can be rewritten as

$$\mathbf{M}_{tot} = \sum_i q_i \cdot \mathbf{r}_{i,cq}, \tag{3.3}$$

where $\mathbf{r}_{i,cq}$ is the centre of charge of a molecule. This expanded version of $\mathbf{M}_{tot}$ is only valid, when talking exclusively about molecular ions, which have a charge, because otherwise one would divide by zero. Furthermore, a centre of charge for the box does not exist, because the sum of

the charge of each molecule i is zero, $\sum_i q_i = 0$.
As already mentioned above the motion of molecules can be split in translation and rotation, the internal motions are included in the rotation.

3.1.2 Translational Moment $\mathbf{M}_J$

The translational moment $\mathbf{M}_J$ [19, 20] can now be written as

$$\mathbf{M}_J = \sum_i q_i \cdot \mathbf{r}_{i,cm}, \tag{3.4}$$

where $\mathbf{r}_{i,cm}$ is the centre of mass.
$\mathbf{M}_J$ is unique too due to the fact that the total charge of all molecules sums up to zero.
$\mathbf{M}_J$ differentiated with respect to the time t results in an electric current $\mathbf{J}(t)$ [21],

$$\begin{aligned}
\mathbf{J}(t) &= \frac{d\mathbf{M}_J}{dt} && (3.5)\\
&= \frac{d}{dt}\sum_i q_i \cdot \mathbf{r}_{i,cm} && (3.6)\\
&= \sum_i q_i \frac{d\mathbf{r}_{i,cm}}{dt} && (3.7)\\
&= \sum_i q_i \cdot \mathbf{v}_{i,cm}, && (3.8)
\end{aligned}$$

where $\mathbf{v}_{i,cm}$ is the centre of mass velocity of a molecule i. $\mathbf{J}(t)$ is, in principle, experimentaly accessible.
In Simulation, however, $\mathbf{M}_J$ suffers from toroidal jumps; A molecule leaves the box on one side and it comes in again on the opposite side with identical centre of mass velocity. The electric current $\mathbf{J}(t)$ does not experience a jump. Therefore, dielectric properties are calculated by means of $\mathbf{J}(t)$ instead of $\mathbf{M}_J$.

3.1.3 Rotational Moment $\mathbf{M}_D$

Now, the rotational part [19] of the total collective dipole moment can be obtained by subtracting $\mathbf{M}_J$ from $\mathbf{M}_{tot}$,

$$\begin{aligned}
\mathbf{M}_D &= \mathbf{M}_{tot} - \mathbf{M}_J && (3.9)\\
&= \sum_i \sum_a q_{i,a} \cdot \mathbf{r}_{i,a} - \sum_i \sum_a q_{i,a} \cdot \mathbf{r}_{i,cm} && (3.10)\\
&= \sum_i \Big(\sum_a q_{i,a} \cdot (\mathbf{r}_{i,a} - \mathbf{r}_{i,cm}) \Big). && (3.11)
\end{aligned}$$

The inner sum of the last equation equals the dipole moment $\boldsymbol{\mu}_i$ of a molecule i,

$$\boldsymbol{\mu}_i = \sum_a q_{i,a}(\mathbf{r}_{i,a} - \mathbf{r}_{i,cm}). \tag{3.12}$$

This equation [22] can also be written in terms of the centre of charge $\mathbf{r}_{i,cq}$ and the centre of mass $\mathbf{r}_{i,cm}$:

$$\begin{aligned} \boldsymbol{\mu}_i &= q_i\left(\frac{\sum_a q_{i,a}\cdot\mathbf{r}_{i,a}}{q_i} - \frac{\sum_a m_{i,a}\cdot\mathbf{r}_{i,a}}{m_i}\right) && (3.13)\\ &= q_i(\mathbf{r}_{i,cq} - \mathbf{r}_{i,cm}) && (3.14)\end{aligned}$$

For interpretation one would like to know the contribution of individual molecular ions to the rotational moment. The last expression allows the splitting of $\mathbf{M}_D$ into a cationic and anionic contribution [22] and we can write

$$\mathbf{M}_D = \mathbf{M}_D^+ + \mathbf{M}_D^- = \sum_i \boldsymbol{\mu}_i^+ + \sum_i \boldsymbol{\mu}_i^-, \tag{3.15}$$

where the superscript + refers to the cations and - to the anions. Since $\mathbf{M}_{tot}$ and $\mathbf{M}_J$ are unique, $\mathbf{M}_D$ is unique too. The molecular contributions $\boldsymbol{\mu}_i^{\pm}$, however, depend on the choice of origin, the centre of mass in the present case.

For the calculation of $\mathbf{M}_D, \mathbf{M}_J$ and $\mathbf{M}_{tot}$ the program *GEPETTO* was used. It was developed by Mag. Michael Haberler, Mag. Gregor Neumayr and Mag. Thomas Taylor, they are all group members. I wrote, in addition, another program to compute $\mathbf{M}_D$ and $\mathbf{M}_J$.

3.2 Correlation Functions

A correlation function [23] can give information about how fast a function $A(t)$ 'loses its memory'. This means that after an amount of time the function $A(t)$ does not know anymore from where it came at the beginning.

The average of the function $A(t)$ should be zero and this condition is fulfilled in equilibrium,

$$\langle A(t)\rangle = 0. \tag{3.16}$$

This expression can also be written in a continous form,

$$\langle A(t)\rangle = \lim_{T\to\infty}\frac{1}{T}\int_0^T A(t)dt, \tag{3.17}$$

The form of a correlation function resembles an inner product of two vectors and is now defined as followed:

$$\big\langle A(\tau) \cdot A(\tau + t) \big\rangle = \lim_{T \to \infty} \frac{1}{T} \int_0^T A(\tau) \cdot A(\tau + t) dt, \tag{3.18}$$

where τ is the initial/reference time of the function and t is the time difference between τ and a later time t. Note, that t is a difference and not a point in time. A correlation function does not change when a different reference time is chosen, due to the fact, that the statistical average is independent of the choice of time origin. Though, good statistics is required. Therefore, a correlation function is independent of the initial time.
Now, it is possible to set $\tau = 0$ and we can write

$$\big\langle A(0) \cdot A(t) \big\rangle = \lim_{T \to \infty} \frac{1}{T} \int_0^T A(0) \cdot A(t) dt. \tag{3.19}$$

The term $\big\langle A(0) \big\rangle$ implies at the same time, that τ is not important. That procedure makes the correlation function stationary with respect to τ, because it is only a function of the time difference t.
The starting point of a correlation function is $\big\langle A(0)^2 \big\rangle$ and then the function decays to the uncorrelated value $\big\langle A \big\rangle$, where $\big\langle A \big\rangle$ is usually zero in equilibrium.
In this thesis the rotational moment $\mathbf{M}_D$ was correlated over time to assess the extend of the relaxation of the molecules. The preferable case is when the correlation function falls down to zero within 1.5 nanoseconds. The correlation function for $\mathbf{M}_D$ is defined as followed:

$$\big\langle \mathbf{M}_D(0) \cdot \mathbf{M}_D(t) \big\rangle = \lim_{T \to \infty} \frac{1}{T} \int_0^T \mathbf{M}_D(0) \cdot \mathbf{M}_D(t) dt \tag{3.20}$$

Please note that it is possible to gain a correlation function, which falls down to zero, if you simulate long enough. Furthermore, the correlation function of the rotational dipole moment is influenced by the dipole momenta of the molecules and their spatial arrangement.
For the calculation of the correlation functions in this thesis, the program *GEPETTO* was used.

3.3 Orientational Probability Functions

The orientational probability function [22, 24–26] $g(r_{ij}, \Omega_i, \Omega_j, \Omega_{ij})$ is used for the analysis of the spatial composition of a structure and is dependent on a distance between two molecular species i and j and on a set of Eulerian angles Ω. Now, the function can be expanded into the rotationally

invariant basis function, so-called angular basis functions $\Phi^{l_i,l_j,l_{ij}}(\Omega_i, \Omega_j, \Omega_{ij})$ [27] [28–30],

$$g_{AB}(r_{ij}, \Omega_i, \Omega_j, \Omega_{ij}) = \sum_{l_i,l_j,l_{ij}} g_{AB}^{l_i,l_j,l_{ij}}(r_{ij}) \cdot \Phi^{l_i,l_j,l_{ij}}(\Omega_i, \Omega_j, \Omega_{ij}), \tag{3.21}$$

where the indices l_i, l_j, l_{ij} give the order of the respective angular momentum. The subscript A refers to reference point and B refers to the point of interest.

For g^{000} the orientational probability function becomes the radial distribution function, which is a molecular property due to the use of the centre of mass of a molecule instead of the atom-atom distance. It gives the probability of finding a molecule i next to another one j at a distance r, this can also be seen as a local density, which is divided by a global density. Furthermore, the angular basis function $\Phi^{l_i,l_j,l_{ij}}$ is one for g^{000} and we can write,

$$g_{AB}^{000}(r) = \frac{\sum_j \langle 1 \cdot \delta(r - |\mathbf{r}_{ij}|)\rangle}{4\pi r^2 dr} \cdot \frac{1}{\rho}. \tag{3.22}$$

For more detailed information about the angular distribution the probability functions of higher angular momenta are needed. The radial distribution function just gives the radial packing, whereas the higher g-coefficients give information on the orientation, too. Therefore, the dipole moment of the molecules i and j are correlated, the local density is weighted with the average cosine of the two dipole moments. The angular basis function Φ^{110} and the corresponding probability function $g^{110}(r)$ are:

$$\Phi^{110} = \frac{\boldsymbol{\mu}_i \cdot \boldsymbol{\mu}_j}{|\boldsymbol{\mu}_i| \cdot |\boldsymbol{\mu}_j|} = \cos(\boldsymbol{\mu}_i, \boldsymbol{\mu}_j) \tag{3.23}$$

$$g_{AB}^{110}(r) = \frac{\sum_j \langle \cos(\boldsymbol{\mu}_i, \boldsymbol{\mu}_j) \cdot \delta(r - |\mathbf{r}_{ij}|)\rangle}{4\pi r^2 dr} \cdot \frac{1}{\rho} \tag{3.24}$$

For $g^{101}(r)$ the radial distribution function is weighted by the cosine of the angle between the distance vector $\mathbf{r}_{ij}$, joining molecular centres, and the dipole moment $\boldsymbol{\mu}_i$ of the molecule i.

$$\Phi^{101} = \frac{\boldsymbol{\mu}_i \cdot \mathbf{r}_{ij}}{|\boldsymbol{\mu}_i| \cdot |\mathbf{r}_{ij}|} = \cos(\boldsymbol{\mu}_i, \mathbf{r}_{ij}) \tag{3.25}$$

$$g_{AB}^{101}(r) = \frac{\sum_j \langle \cos(\boldsymbol{\mu}_i, \mathbf{r}_{ij}) \cdot \delta(r - |\mathbf{r}_{ij}|)\rangle}{4\pi r^2 dr} \cdot \frac{1}{\rho} \tag{3.26}$$

$g^{011}(r)$ it is defined as the analogue of $g^{101}(r)$. Here, the distance vector $\mathbf{r}_{ij}$ is correlated with the dipole moment of the molecule j:

$$\Phi^{101} = \frac{\boldsymbol{\mu}_j \cdot \mathbf{r}_{ij}}{|\boldsymbol{\mu}_j| \cdot |\mathbf{r}_{ij}|} = \cos(\boldsymbol{\mu}_j, \mathbf{r}_{ij}) \tag{3.27}$$

$$g_{AB}^{101}(r) = \frac{\sum_j \left\langle \cos(\boldsymbol{\mu}_j, \mathbf{r}_{ij}) \cdot \delta(r - |\mathbf{r}_{ij}|) \right\rangle}{4\pi r^2 dr} \cdot \frac{1}{\rho} \tag{3.28}$$

The higher g-coefficients involve polynomials of higher degree in the direction of the cosines. All these functions can be computed by means of *GEPETTO*.
Furthermore, a so-called charge ordering function $g_\Delta(r)$ can be calculated out of g_{++}^{000}, g_{--}^{000} and g_{+-}^{000}, where the subscript + refers to the cations and - the anions:

$$g_\Delta(r) = g_{+-}^{000}(r) - \frac{1}{2}\Big(g_{++}^{000}(r) + g_{--}^{000}(r)\Big) \tag{3.29}$$

The more the charges are ordered, the longer the function will oscillate around zero on a radial scale.

4 BMIM_TRIF_891

The aim of this thesis was to discover an efficient way to generate good starting structures and the following assessment of these newly created configurations.

Therefore, the model system, consisting of the cation 1-Butyl-3-methyl-imidazolium (BMIM) and the anion Triflate (TRIF), was chosen on purpose. BMIM is as a cation (Fig. 4.1) quite flat, due to the Imidazolium-ring, but it has a capacious diameter. Furthermore it is the largest cation investigated by the group. The anion (Fig. 4.2) has a shape of a cylinder and was also chosen because of its dimensions. According to the experimental density, 891 ion pairs were packed together in a 69Å-box.

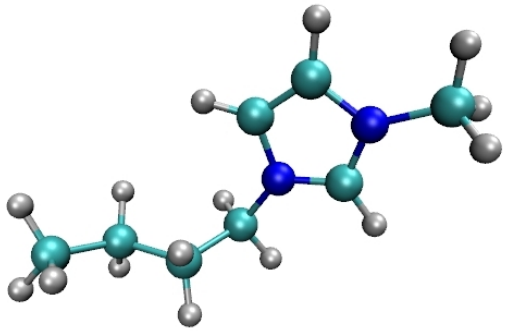

Figure 4.1: The cation 1-Buthyl-3-methyl-imidazolium (BMIM)

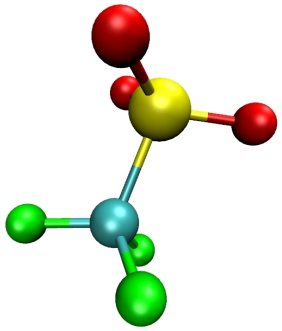

Figure 4.2: The anion Triflate (TRIF)

The general procedure was:

All configurations were packed with the program package PACKMOL. Then the next steps were carried out by CHARMM. First the energy was minimized, followed by the adjustment of the box length, if necessary, because various systems were assigned into too large boxes. At many occasions, the SCALAR-command was used on the charges of the atoms for the adjustment of the box length. As a last step simulation was done. All systems were simulated for 1.5 nanoseconds with a time step of 0.001 picoseconds. The Particle-Mesh-Ewald method [31] was used for the computation of the electrostatics. Therefore, the gridsize was set to 1.08Å, cappa was 0.41 and a spline-order of 6 was chosen. Coordinate files were printed out every 50 picoseconds. The

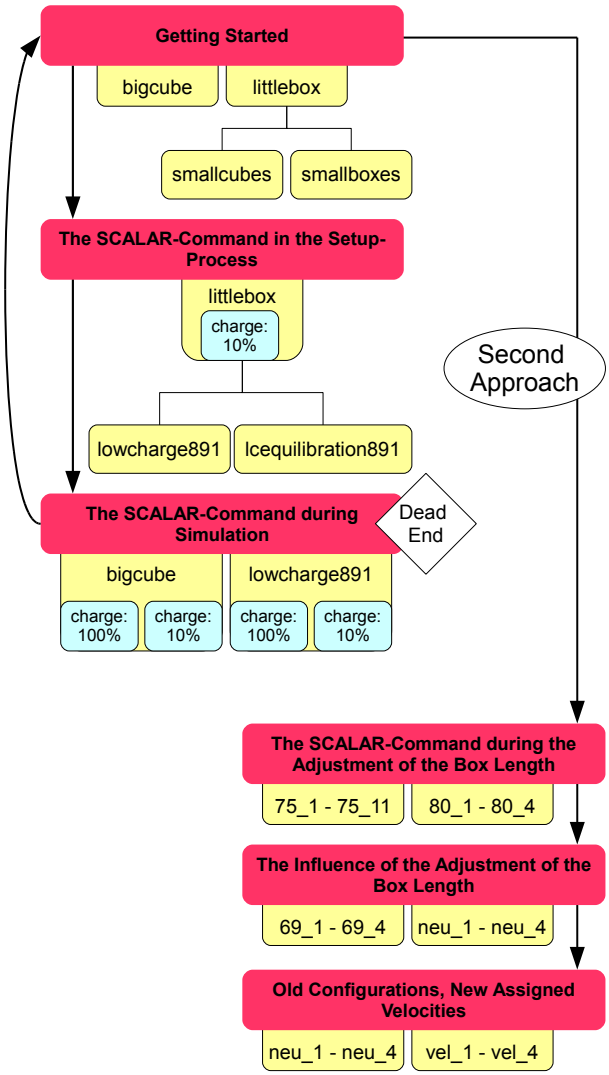

Figure 4.3: The approach for finding a 'good' starting structure.

coordinate files were needed for the calculation of the instantaneous values for the rotational moment $\mathbf{M}_D$.

In Fig. 4.3 the reader can see the approach for finding a 'good' starting structure as a diagram for better understanding. The text in the red boxes refers to the caption of the next sections and the yellow boxes give the names of the systems.

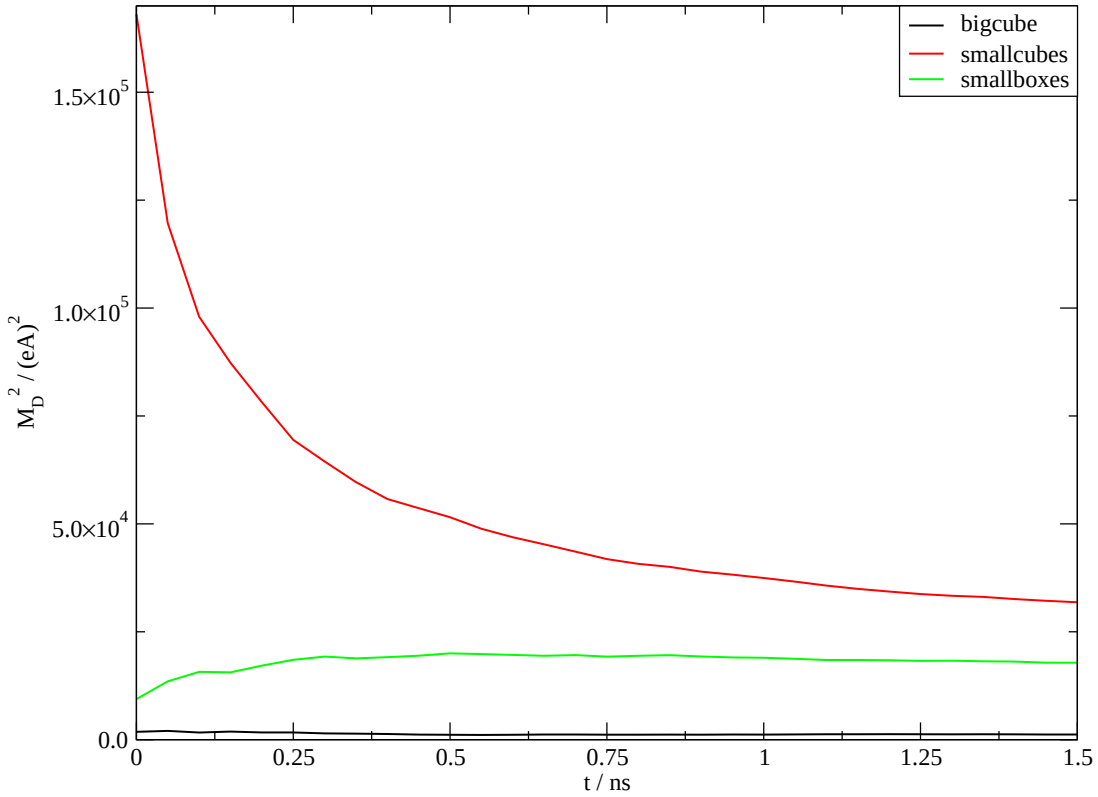

Figure 4.4: The cumulative averaged values of $\mathbf{M}_D^2$ of *bigcube*, *smallcubes* and *smallboxes*. *smallcubes* and *smallboxes* were both too high in their values.

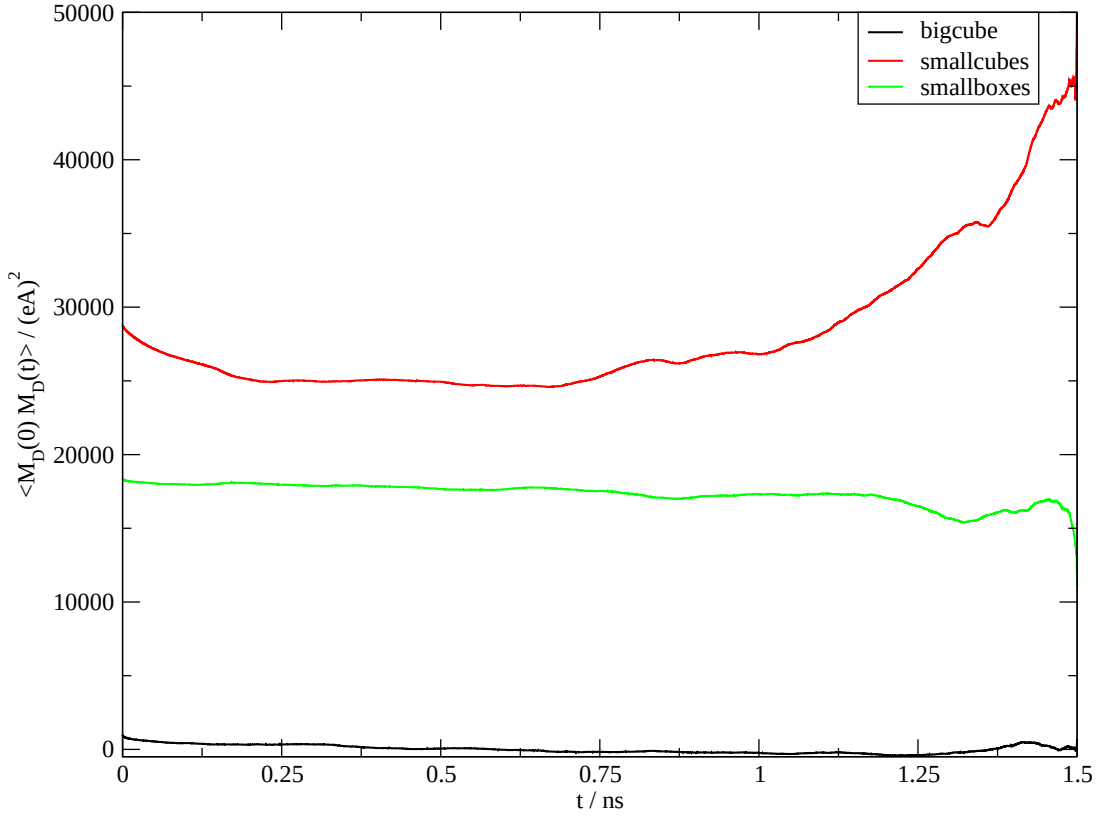

Figure 4.5: The correlation functions for $\mathbf{M}_D$ of *bigcube*, *smallcubes* and *smallboxes*.

4.1 Getting Started

Name	# of Ion Pairs	Box length(Å)	Using SCALAR
bigcube	891	80	yes
littlebox	33	30	yes

Table 4.1: The systems packed by PACKMOL. *littlebox* was needed for the generation of the systems *smallcubes* and *smallboxes*.

Bigcube was the first system to test PACKMOL. The adaption of the box length took quite a long time, therefore a new, smaller system *littlebox* was packed (Table 4.1). After the adjustment, *littlebox* was put into the program *cubebuilder*, which duplicates the cube in all three dimensions. That way, the system *smallcubes* was obtained.

For the system *smallboxes littlebox* was equilibrated to find the conformation with the smallest $\mathbf{M}_D$. That conformation was put in the *cubebuilder*.

In Fig. 4.4 the cumulative averaged values of $\mathbf{M}_D^2$ of the systems *bigcube*, *smallcubes* and *smallboxes* are recorded. The values of *bigcube* were the lowest. For *smallcubes* the $\mathbf{M}_D^2$ values were far too high. This was due to the duplication, in doing so the system was more ordered. Thus *littlebox* was equilibrated to find the conformation with the smallest $\mathbf{M}_D^2$. The outcome of this was *smallboxes*. On the one hand, the rotational moment was lower than for *smallcubes*, but on the other hand the equilibration of *littlebox* needed time too. As another disadvantage, *smallboxes* was a worse system as compared to *bigcube*. The examination of the correlation functions (Fig. 4.5) provided us with the same disappointing results. The correlation function of *smallcubes* had the highest values, followed by *smallboxes* and then *bigcube*.

Since the values of the rotational moment were promising, *bigcube* became the reference system. The generation of a system by duplicating a smaller cube in all three dimension, does not provide satisfying results. Even the equilibration of *littlebox*, before the construction of *smallboxes*, does not have the desireable outcome. But reducing the charge during the equilibration of *littlebox* may give better results.

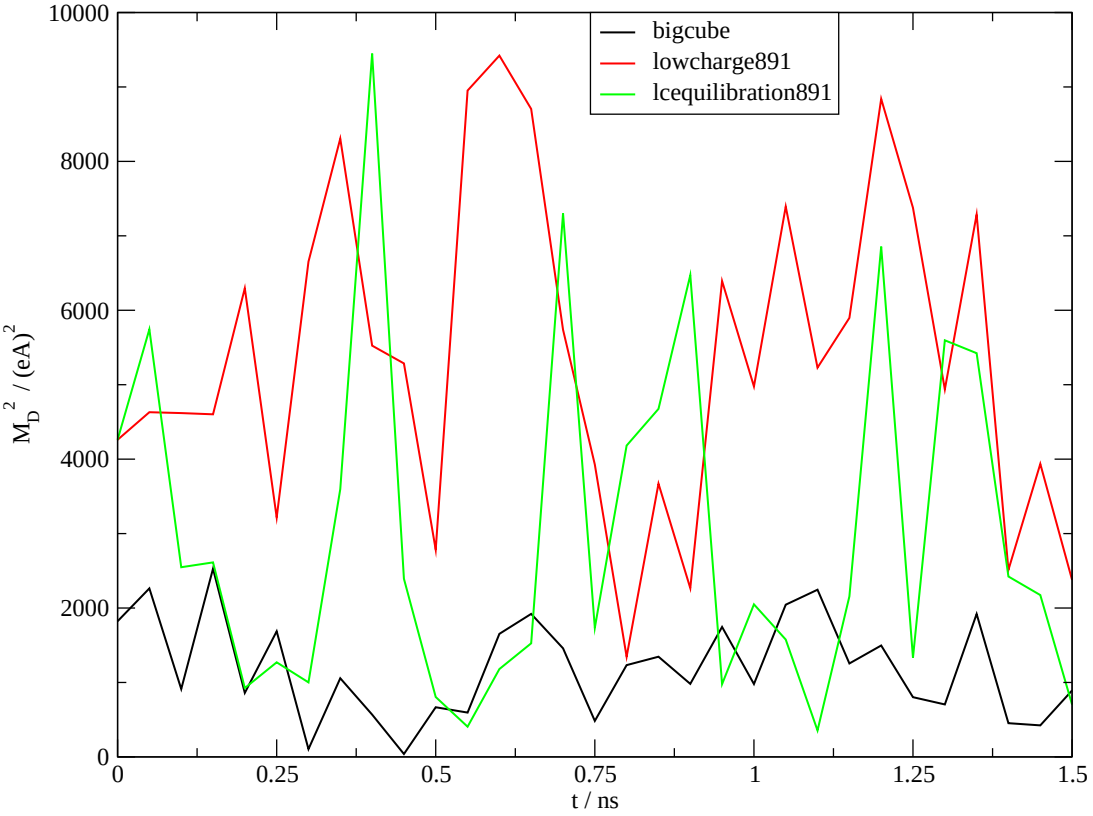

Figure 4.6: The instantaneous values of $\mathbf{M}_D^2$ of *bigcube*, *lowcharge891* and *lcequilibration891*. The values of *lowcharge891* did not even get close to those of *bigcube*. The values of *lcequilibration891* declined quick to those of *bigcube*, but they had a lot of outliers too.

4.2 The SCALAR-Command in the Setup Process

The charges of the system *littlebox* were scaled to 10% of the original values and then equilibrated. The conformation with the smallest $\mathbf{M}_D$ was put into the cubebuilder and the systems *lowcharge891* and *lcequilibration891* (lc stands for low charge) were obtained. Note, that both systems have the same start configuration, which can be seen in Fig. 4.6, but they differ in the following simulation. *Lowcharge891* was simulated with the normal set of charges and *lcequilibration891* with just 10% of the original values. The instantaneous values of $\mathbf{M}_D^2$ of *bigcube*, *lowcharge891* and *lcequilibration891* are plotted in Fig. 4.6. The values of *lowcharge891* were far too high.

The values of *lcequilibration891* instead declined quick to those of *bigcube*, but the values for the rotational moment $\mathbf{M}_D^2$ jumped a lot. Although, the correlation function of *lcequilibration891* (Fig. 4.7) looked promising, the way of production cannot be applied. The reasons are given in the chapter 4.3. The correlation function of *lowcharge891* is not good enough.

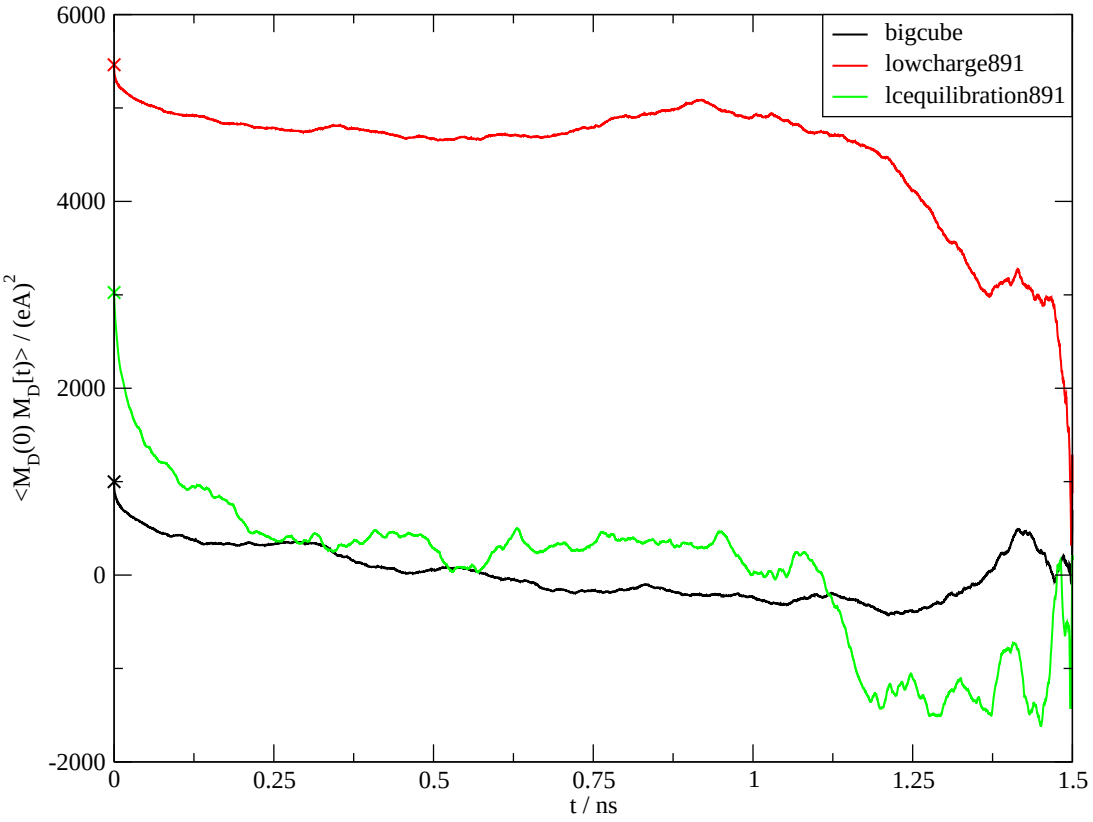

Figure 4.7: The correlation functions for $\mathbf{M}_D$ of *bigcube*, *lowcharge891* and *lcequilibration891*. Although *lcequilibration891* looks promising it cannot be used, because simulation with scaled charges to just 10% of the original values affects the radial distribution function (see Fig. 4.8). The correlation function of *lowcharge891* is still not good enough.

Nevertheless, both systems were better than *smallcubes* and *smallboxes*. The simulation with a scaled set of charges requires a further investigation of the structures.

4.3 The SCALAR-Command during Simulation

After one nanosecond of equilibration, the simulation of *bigcube* was split up into two simulations, which differ in the setting of the charges. The first simulation was done with the normal set of charges and for the second simulation the charges were rescaled to just 10% of the original values. The same was done for *lowcharge891*.

Note, that *lcequilibration891* was also simulated with charges, which were scaled to 10%.

The simulation with just 10% of the original values for the charges reduces the electrostatic interactions and the ions move closer to each other. This results in different radial distribution functions and can be seen in Fig. 4.8. The systems, which were simulated with less charge, can be found at shorter distances than those simulated with the original set of charges.

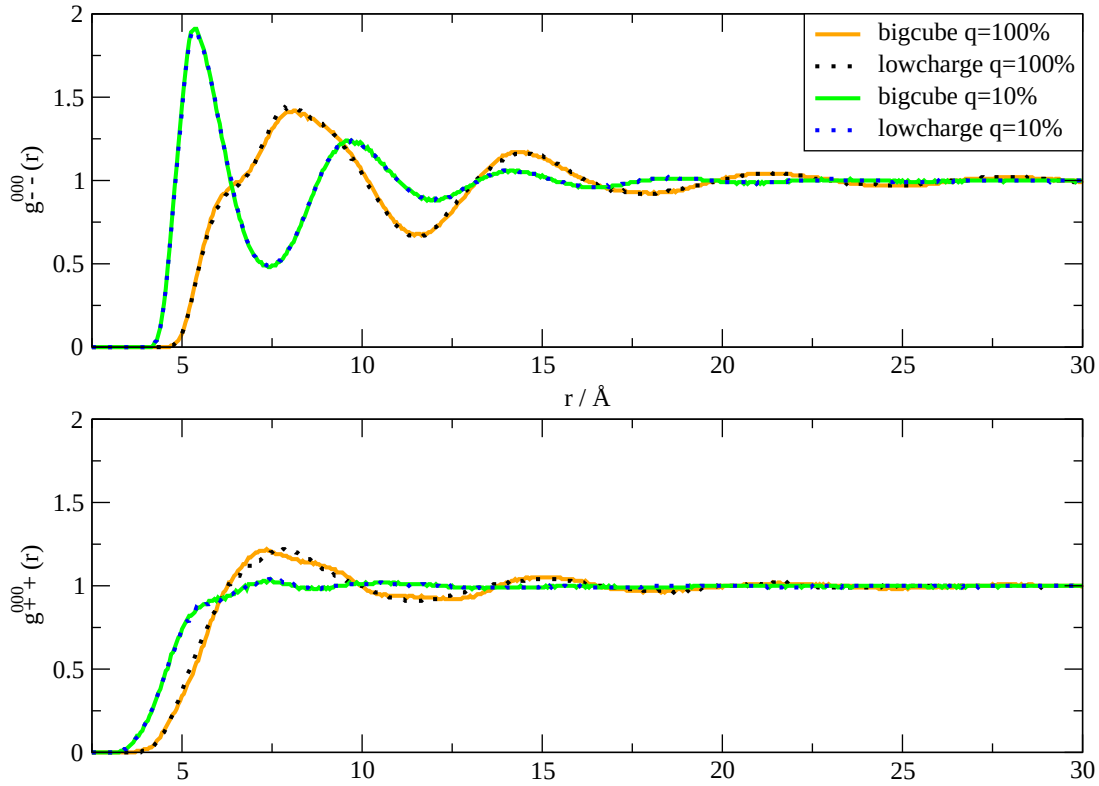

Figure 4.8: In the upper graph the anion was the reference point and the point of interest of the radial distribution function. The same goes for the cation for the lower graph. In both graphs the systems with just 10% of the charges can be found at shorter distances than those with the original set of charges. (q stands for the charge)

That means, that the simulation with 10% of the charges is not admissible, due to the modified electrostatics.

4.4 The SCALAR-Command during the Adjustment of the Box Length

To be able to pack boxes with the same number of ion pairs and the same box length, but a different conformation, i.e. another spatial arrangement, PACKMOL asks for the parameter *seed*. This parameter is a number and can have any value of an integer (Table 4.2). The default for seed is 191917.

To assess the influence of the SCALAR-command during the resizing process, the systems *75_1* - *75_10* were packed. The adjustment of the box length was done by the use of the SCALAR-command on the charges of the atoms. At the beginning the charges were scaled to just 10% of the original values. During the shrinking process the charges were rescaled to the original values. It took about 35 times 10000 steps constant pressure dynamics. One step resembles 0.001 picoseconds. For *75_11* no scaling was done and the experimental density was reached

Name	# of Ion Pairs	Box length(Å)	Using SCALAR	seed
75_1	891	75	yes	1
75_2	891	75	yes	7
75_3	891	75	yes	23
75_4	891	75	yes	58
75_5	891	75	yes	109
75_6	891	75	yes	211
75_7	891	75	yes	237
75_8	891	75	yes	497
75_9	891	75	yes	322
75_10	891	75	yes	87
75_11	891	75	no	3
80_1	891	80	no	500
80_2	891	80	no	507
80_3	891	80	no	702
80_4	891	80	no	913

Table 4.2: The systems for the assessment of the SCALAR-command during the resizing process. *Seed* refers to the seed in PACKMOL, which is needed for the setup of different boxes.

after 26 times 10000 steps dynamics. This result was very promising and *80_1 - 80_4* were packed. Again it just took about 25 times 10000 steps for the shrinking process. This meant a great deal of time saving.

4.5 The Influence of the Adjustment of the Box Length

Name	# of Ion Pairs	Box length(Å)	seed
69_1	891	69	1
69_2	891	69	20
69_3	891	69	43
69_4	891	69	67
neu_1	891	69	1
neu_2	891	69	20
neu_3	891	69	43
neu_4	891	69	67

Table 4.3: This are the systems needed for the assessment of the influence of resizing process together with systems of Table 4.2. Actually, *neu_1 - neu_4* were packed in exactly the same manner as *69_1 - 69_4*, but this time the coordinate system was relocated.

A general examination of the correlation functions of various systems was done to assess the influence of the resizing process (Fig. 4.9 - Fig. 4.13). Furthermore, four conformations, *69_1 - 69_4*, were packed in a 69Å-box (Table 4.3). After a visual examination, I found out that all the boxes of the systems *69_1 - 69_4*, *75_1 - 75_11* and *80_1 - 80_4* had holes in it. These holes appeared after the minimization of the energy, but disappeared after the first 10000 steps of

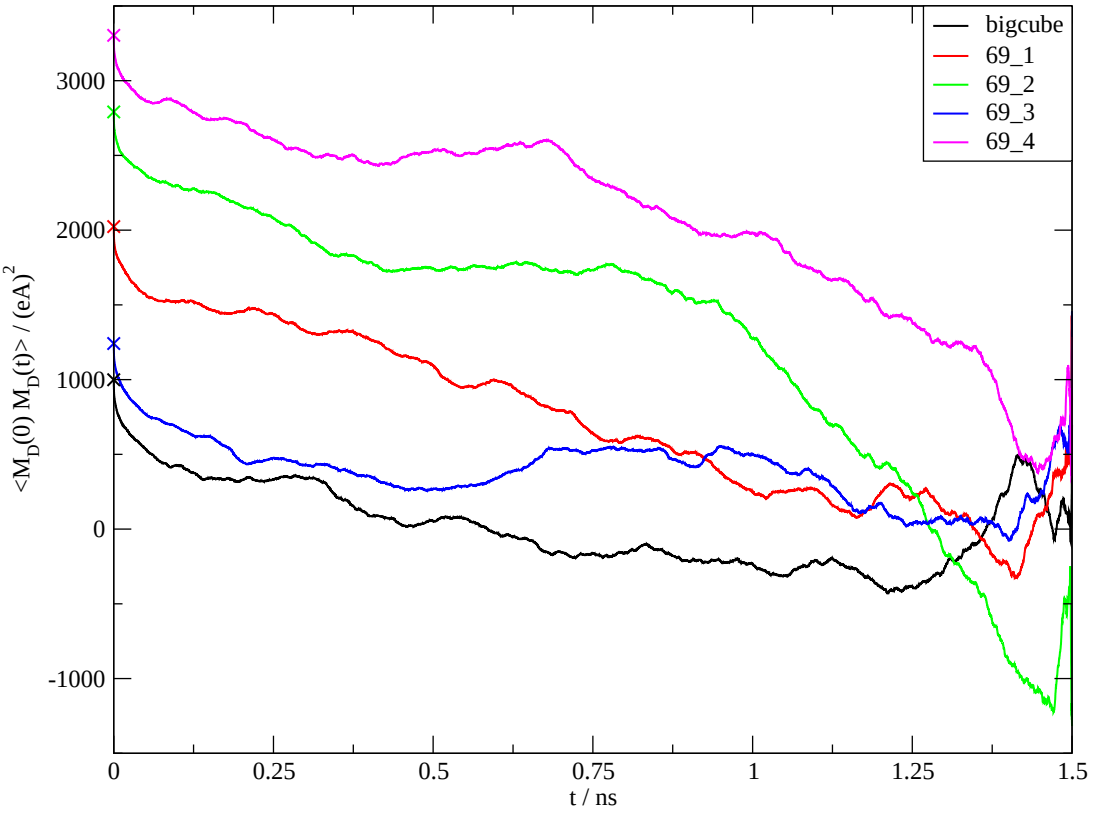

Figure 4.9: The correlation functions for $\mathbf{M}_D$ of *bigcube* and *69_1 - 69_4*.

dynamics. The holes came into existence, due to the fact, that PACKMOL assigns the molecules into a box with a different coordinate system than CHARMM. In the program PACKMOL the origin of the coordinate system can be found at (0/0/0) and the three axes end at the length of the box. In CHARMM the origin is in the middle of the box and it divides x-, y- and z-axis in half. For the systems *neu_1 - neu_4* the coordinate system of *69_1 - 69_4* was relocated before the minimization. That procedure prevented the appearance of holes.

Packing the molecules into bigger boxes, than necessary, does not make it more likely that the rotational moment $\mathbf{M}_D$ relaxes better (Fig. 4.9 - Fig. 4.13). Therefore one can save time by packing the ions directly into a box according to the experimental density.

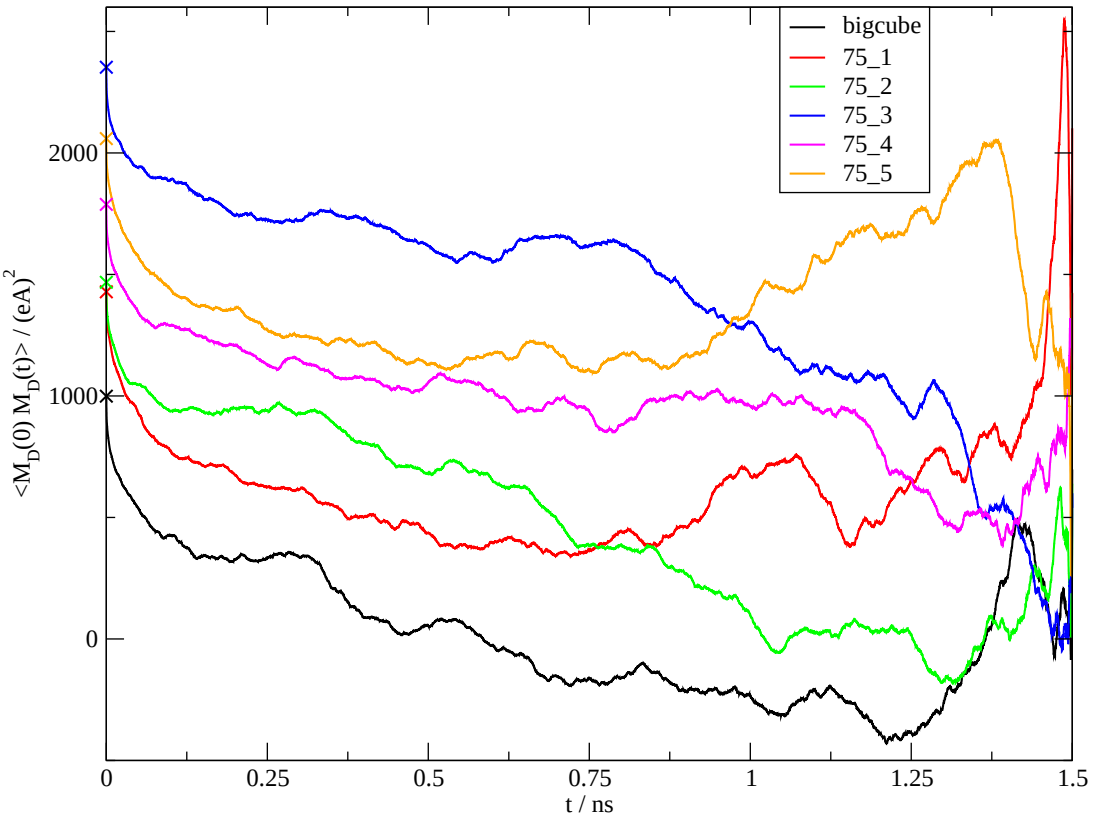

Figure 4.10: The correlation functions for $\mathbf{M}_D$ of *bigcube* and *75_1 - 75_5*.

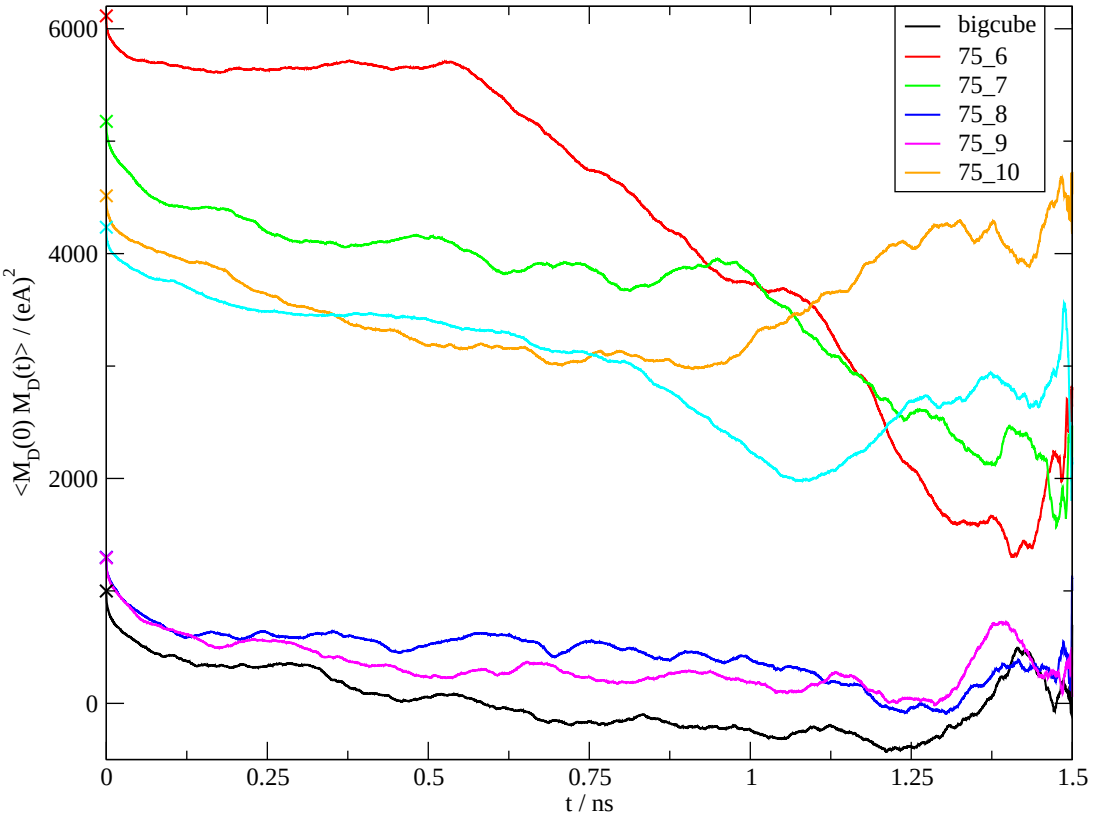

Figure 4.11: The correlation functions for $\mathbf{M}_D$ of *bigcube* and *75_6 - 75_10*.

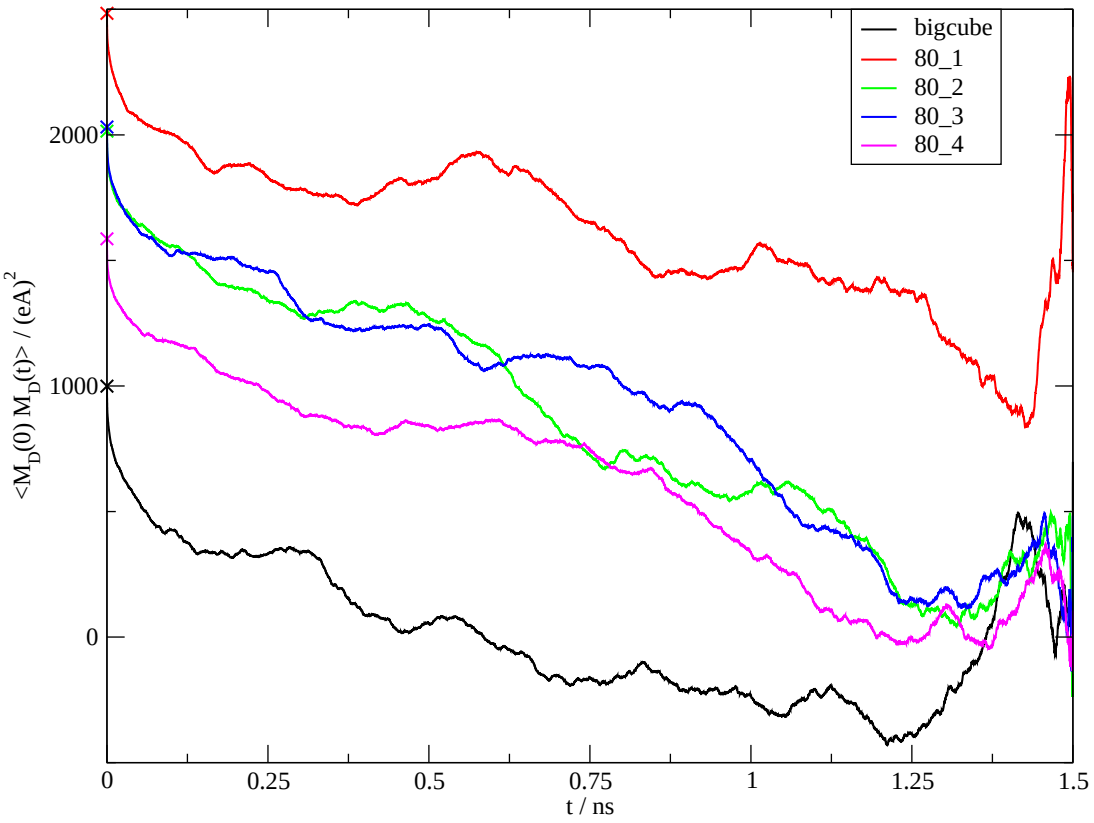

Figure 4.12: The correlation functions for $\mathbf{M}_D$ of *bigcube* and *80_1 - 80_4*.

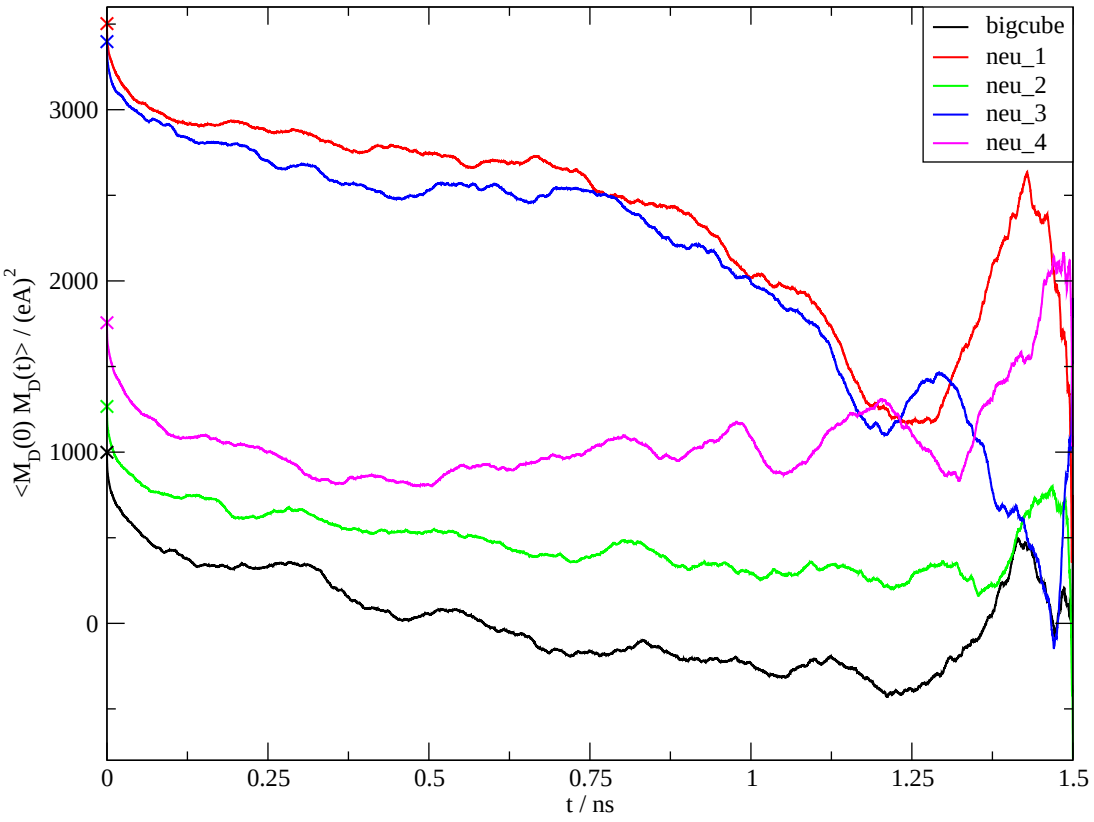

Figure 4.13: The correlation functions for $\mathbf{M}_D$ of *bigcube* and *neu_1 - neu_4*.

4.6 Old Configurations, New Assigned Velocities

Name	iseed
vel_1	234
vel_2	835
vel_3	730
vel_4	591

Table 4.4: The systems of *vel_1 - vel_4* with the value for *iseed*. They are actually the systems *neu_1 - neu_4* just simulated with a different *iseed*.

The same minimized structures of *neu_1 - neu_4* were equilibrated again, but this time other velocities were assigned for the dynamics. The user has the possibility to do this by the use of the option *iseed* in CHARMM. This is an integer for the random number generator, which is used for assigning velocities, and the default is 314159. With a value for *iseed*, the velocities are distributed according to a Gauss distribution.

In principle there exist other distributions too, which are chosen with the option *iasvel*. For the value 1, the default, it is a Gauss distribution, for -1 it is a uniform distribution and for the value zero the velocities are assigned by the comparison coordinate set.

The new systems had the names *vel_1 - vel_4* and the values for the corresponding *iseed* can be found in Table 4.4.

In Fig. 4.14 and 4.15 one can see the instantanious values of $\mathbf{M}_D^2$ for the systems *neu_1 - neu_4* and *vel_1 - vel_4*. It is apparent, that the values of the graph *neu_1* (Fig. 4.14) jump a lot, as do the values for *vel_1*. For *neu_2* the values range in a smaller region and they do not jump as much. The same trend can be seen in the corresponding system *vel_2*. The same behaviour can be observed for *neu_3* and *neu_4* with *vel_3* and *vel_4* in Fig. 4.15.

Next, the correlation functions were examined in Fig. 4.16 and Fig. 4.17. The correlation function of *neu_2* and *vel_2* are nearly the same. Furthermore, they provide the best reults. The other correlation functions are not as good as those. Moreover, one can see that a 'bad' structure does not get better, when simulating it with other velocities. They may differ from each other, but they would not get better. Thus, one can say, that the relaxation of the rotational moment $\mathbf{M}_D$ is independent of the assigned velocities. It is only constrained to the spatial arrangement and/or composition.

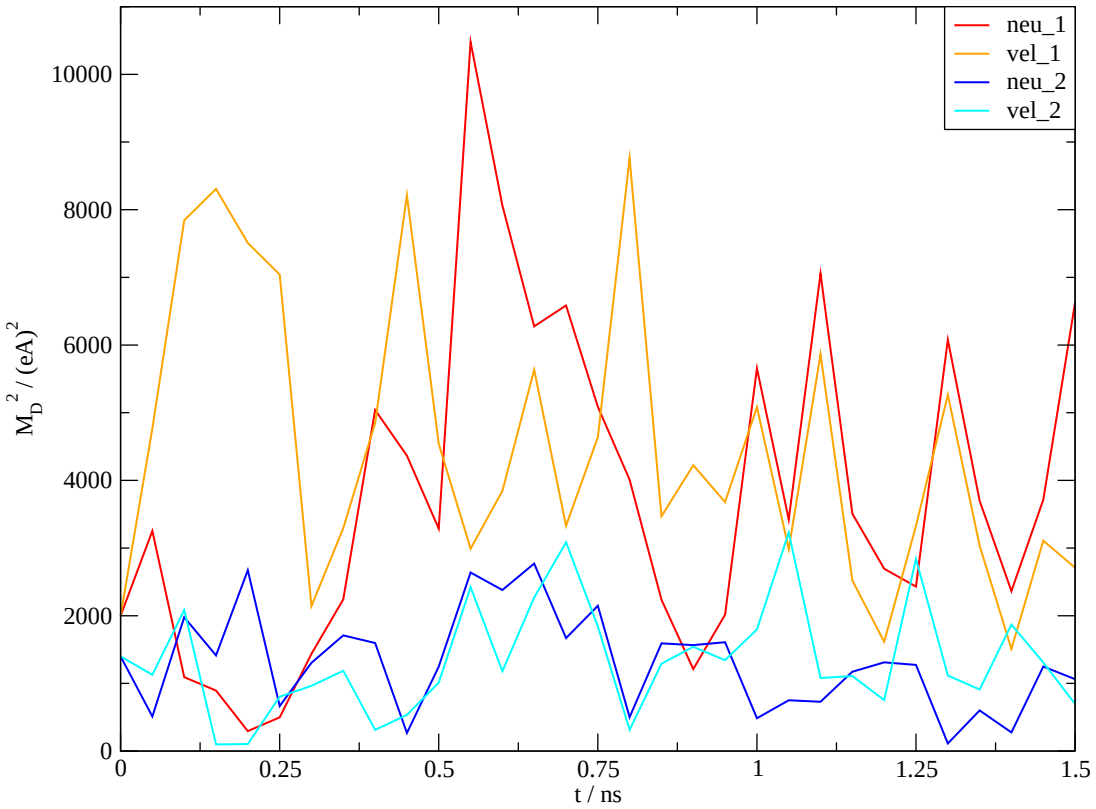

Figure 4.14: The instantaneous values of $\mathbf{M}_D^2$ of *neu_1* with the corresponding values of *vel_1*. The same goes for *neu_2* and *vel_2*.

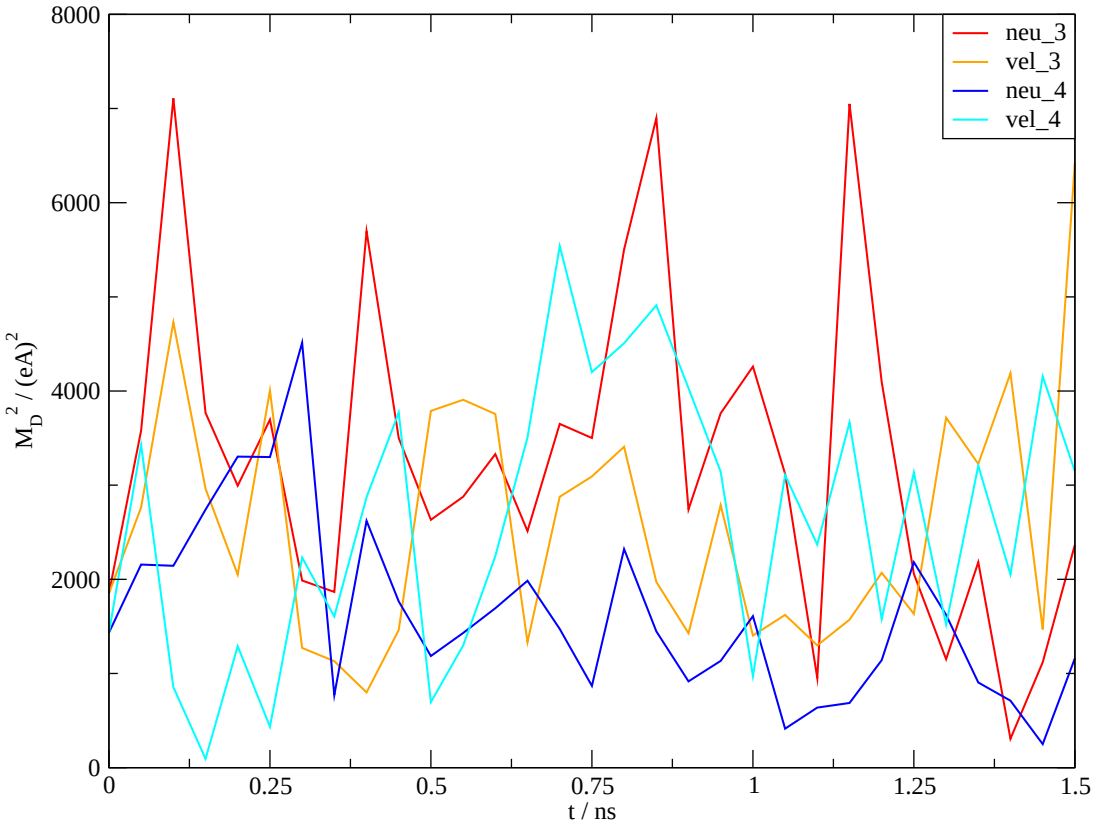

Figure 4.15: The instantaneous values of $\mathbf{M}_D^2$ of *neu_3* with the corresponding values of *vel_3*. The same goes for *neu_4* and *vel_4*.

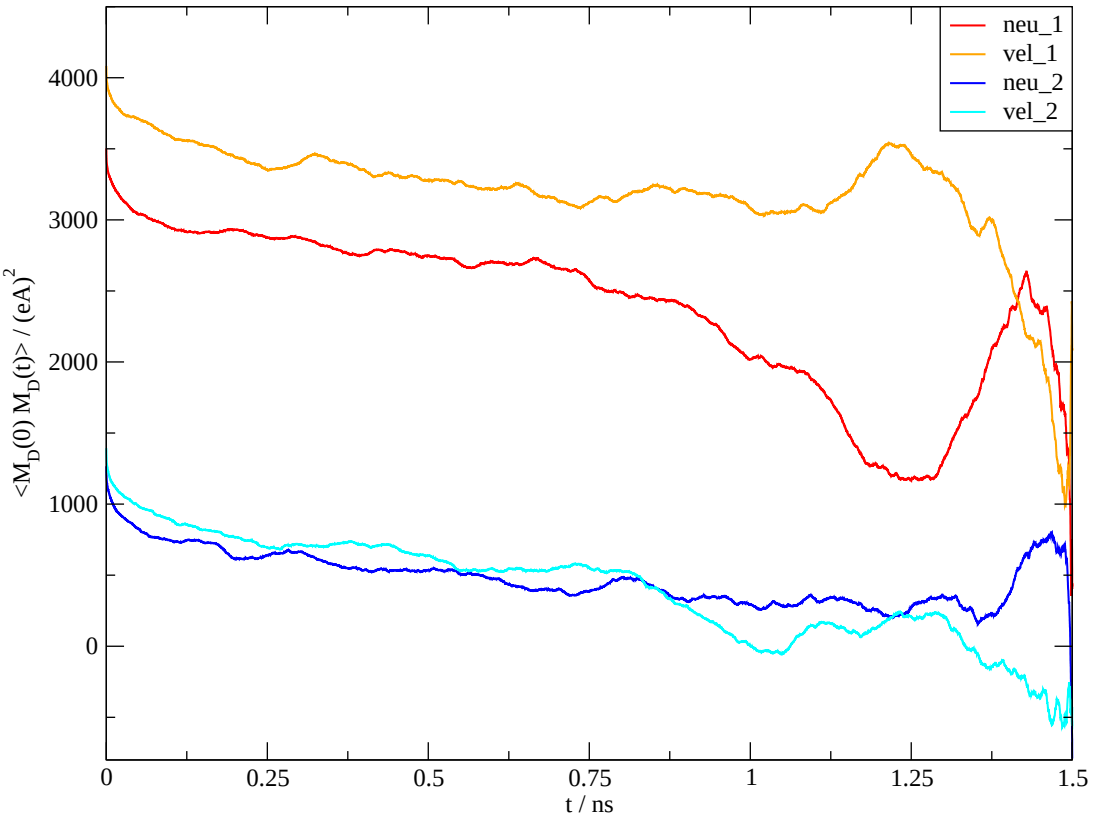

Figure 4.16: The correlation functions of *neu_1*, *neu_2* and *vel_1*, *vel_2*. The functions of *neu_2* and *vel_2* are the best of these systems and they do not differ much from each other.

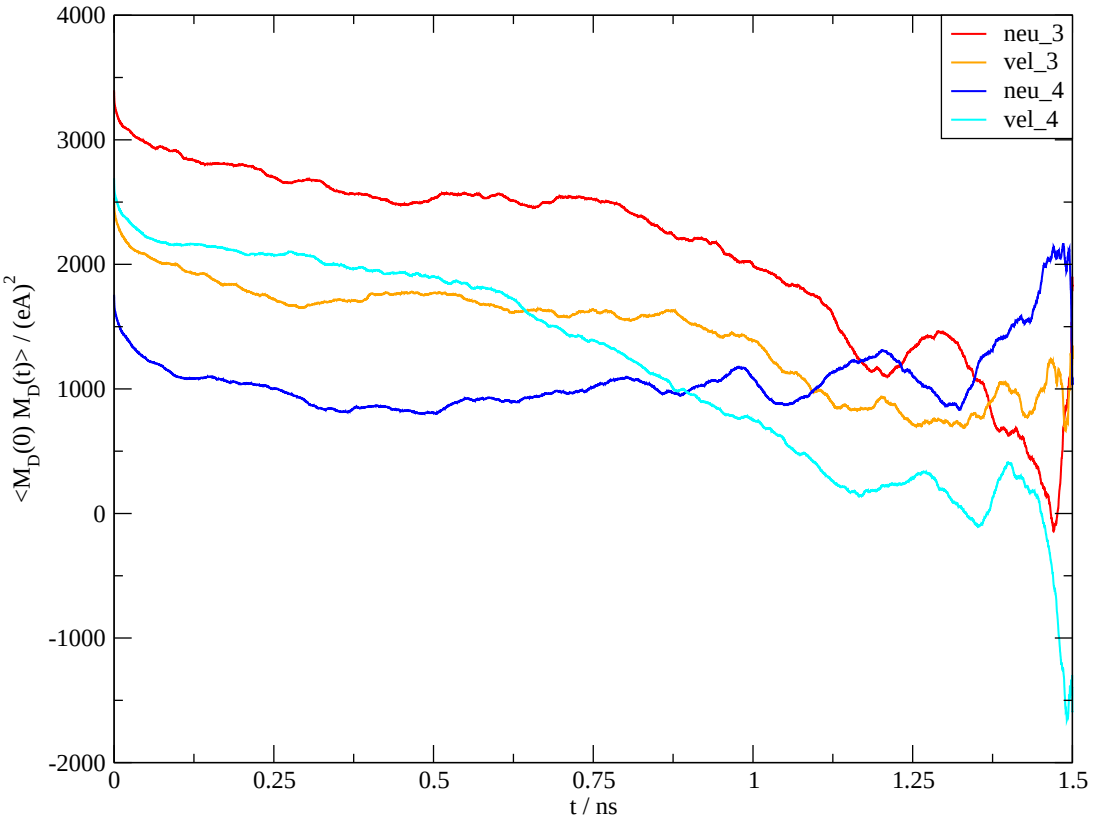

Figure 4.17: The correlation functions of *neu_3*, *neu_4* and *vel_3*, *vel_4*. All systems are worse than *neu_2* and *vel_2*.

5 Investigation of the Spatial Composition

After the discovery that the relaxation of a system is dependent on its spatial composition, an evaluation of the structures themselves, which are used at the beginning of the equilibration, was of interest.

5.1 Homogeneity of the Boxes

First, the homogeneity of the boxes was tested. Therefore a program divides the box of interest in 27 sub-boxes, two divisions in each dimension. This partition was chosen with regard to the dimensions of the molecules. Is the sub-box to small, the values for the rotational moment have no significance.

As representatives the systems *bigcube*, *neu_1*, *neu_2* and *neu_3* were chosen. The correlation functions of *bigcube* and *neu_2* are examples of structures, which show a good relaxation, while *neu_1* and *neu_3* do not (Fig. 4.13). Of these systems the components of the rotational moment $\mathbf{M}_D$, the square of the rotational dipole moment $\mathbf{M}_D^2$, which is a scalar, and the number of cations and anions of each sub-box was calculated (Table 5.1 - Table 5.4). Note, that the summation of $\mathbf{M}_D^2$ over all sub-boxes does not to equal the total rotational dipole moment squared.

The comparison of the average values of $\mathbf{M}_D^2$ of Table 5.1 - Table 5.4 did not give any trend. The system *bigcube* had the smallest value with $99.71(eA)^2$ followed by *neu_3* with $163.97(eA)^2$. But *neu_3* is a structure, which does not relax well. The next best value, $175.10(eA)^2$, is from *neu_2*, a 'good' structure. The worst value is from *neu_1* with $204.36(eA)^2$, again a 'bad' structure. Furthermore, the ions were well distributed over all sub-boxes in all systems. To gain a deeper insight in the spatial arrangement another approach was necessary.

Name	box	$\mathbf{M}_D^x$	$\mathbf{M}_D^y$	$\mathbf{M}_D^z$	$\mathbf{M}_D^2$	# of cations	# of anions
bigcube	1	-2.42	-3.70	1.76	22.60	30	29
	2	-2.86	-5.92	7.54	100.04	36	30
	3	-3.27	-1.84	-4.95	38.62	27	33
	4	8.39	0.22	4.27	88.67	37	34
	5	7.31	5.41	-8.05	147.46	34	33
	6	-5.91	3.83	5.58	80.67	32	32
	7	-5.91	3.83	5.58	80.67	32	32
	8	0.88	-2.96	2.04	13.7	32	33
	9	6.37	8.14	6.85	153.8	34	32
	10	-4.81	12.97	6.46	232.96	35	33
	11	-1.58	-2.96	6.20	49.73	29	37
	12	-5.39	-0.35	-15.36	264.97	32	31
	13	-7.54	-11.79	-2.51	201.98	35	33
	14	10.50	1.86	-5.07	139.43	34	33
	15	-3.32	3.92	-7.42	81.35	35	35
	16	-8.17	1.00	9.59	159.68	33	38
	17	3.55	6.17	0.87	51.43	32	32
	18	-0.97	5.66	16.07	291.33	29	35
	19	-1.26	4.31	-1.53	22.54	32	35
	20	-3.44	-1.75	2.82	22.88	37	34
	21	-6.79	1.03	-3.36	58.46	37	32
	22	2.36	-3.66	6.09	56.11	34	31
	23	-1.29	1.12	-14.61	216.41	33	35
	24	-1.33	1.25	5.56	34.20	31	32
	25	-1.68	-3.48	-3.90	30.08	31	35
	26	-4.70	-2.17	1.85	30.17	33	32
	27	-1.05	6.02	-4.46	57.31	36	30
average		-1.05	1.07	0.51	99.71	33	33
σ		4.81	5.12	7.18	81.6	2.6	2.08

Table 5.1: The investigation of the homogeneity of *bicube*, a 'good' structure.

Name	box	$\mathbf{M}_D^x$	$\mathbf{M}_D^y$	$\mathbf{M}_D^z$	$\mathbf{M}_D^2$	# of cations	# of anions
neu_2	1	0.90	-5.21	-6.47	69.78	27	34
	2	4.60	-3.33	-2.62	39.14	33	34
	3	-10.21	-1.79	-1.33	109.28	26	28
	4	-3.47	-1.43	3.92	29.41	30	34
	5	8.32	1.26	-2.98	79.66	40	34
	6	-5.07	0.53	5.78	59.35	35	32
	7	-6.16	-3.26	-7.79	109.23	30	33
	8	-5.35	10.22	-4.52	153.55	34	36
	9	-3.82	15.64	1.54	261.49	29	26
	10	-4.51	2.96	-2.70	36.39	30	35
	11	-12.12	-11.42	-6.54	319.90	40	32
	12	-1.04	-3.75	-3.32	26.16	35	34
	13	1.31	-1.16	5.79	36.55	41	36
	14	2.58	9.83	-5.62	135.01	35	34
	15	-6.21	2.75	4.46	65.98	35	35
	16	-8.44	-8.19	4.22	156.15	35	32
	17	4.86	2.27	7.17	80.14	36	36
	18	6.50	19.01	0.96	404.52	31	35
	19	-0.90	8.06	-8.03	130.34	30	32
	20	16.39	-7.55	-1.28	327.35	34	32
	21	5.29	-15.98	13.78	473.14	31	30
	22	-6.01	1.86	8.55	112.69	30	33
	23	5.18	7.72	-14.06	284.19	29	33
	24	22.24	-3.81	11.33	637.37	38	33
	25	21.10	0.65	3.76	459.87	36	33
	26	1.45	-6.03	4.68	60.35	30	33
	27	5.28	6.52	-0.67	70.83	31	32
average		1.21	0.61	0.30	175.10	33	33
σ		8.68	7.90	6.50	163.57	3.97	2.23

Table 5.2: The investigation of the homogeneity of *neu_2*, a 'good' structure.

Name	box	$\mathbf{M}_D^x$	$\mathbf{M}_D^y$	$\mathbf{M}_D^z$	$\mathbf{M}_D^2$	# of cations	# of anions
neu_1	1	-1.11	2.81	-12.40	162.94	27	28
	2	-5.06	-0.23	-9.55	116.84	37	39
	3	4.26	1.17	7.74	79.46	27	26
	4	10.54	-4.10	-5.86	162.30	38	35
	5	-10.41	-5.04	-4.48	153.93	33	36
	6	1.63	1.96	9.77	101.96	26	38
	7	-5.56	7.41	-12.32	237.53	26	32
	8	3.34	2.22	-13.82	206.94	37	32
	9	-5.40	4.45	8.83	126.99	30	28
	10	-6.74	5.65	-3.00	86.43	30	29
	11	-5.75	-4.76	-1.06	56.90	34	35
	12	0.95	-2.81	9.62	101.33	33	31
	13	-6.58	-15.47	-4.77	305.23	33	34
	14	-1.05	-3.08	-7.84	72.05	37	37
	15	-13.82	9.57	10.92	401.84	39	35
	16	-5.94	7.19	-13.17	260.50	34	32
	17	-8.37	5.66	0.52	102.45	36	34
	18	0.79	5.75	7.08	83.74	34	32
	19	6.66	-10.37	-1.79	155.19	28	31
	20	14.50	-3.12	0.36	219.98	31	34
	21	14.23	-7.62	3.63	273.64	35	35
	22	-7.85	7.25	-9.72	208.66	34	35
	23	14.17	-2.62	1.76	210.68	35	35
	24	16.46	6.00	18.50	649.00	35	32
	25	12.04	-5.22	-22.51	678.81	32	32
	26	7.16	4.27	10.74	184.71	39	30
	27	10.17	0.22	3.79	117.77	31	34
average		1.23	0.26	-1.08	204.36	33	33
σ		8.79	6.10	9.74	155.18	3.88	3.11

Table 5.3: The investigation of the homogeneity of *neu_1*, a 'bad' structure.

Name	box	$\mathbf{M}_D^x$	$\mathbf{M}_D^y$	$\mathbf{M}_D^z$	$\mathbf{M}_D^2$	# of cations	# of anions
neu_3	1	-3.31	-12.63	0.53	170.70	30	28
	2	-9.94	0.47	4.34	117.86	30	32
	3	-5.76	-4.41	-3.84	67.37	28	31
	4	-17.72	9.65	-9.06	489.17	30	36
	5	-6.69	-1.80	1.85	51.38	32	32
	6	-6.99	-5.31	6.22	115.69	33	27
	7	-1.43	-3.32	0.05	13.06	27	30
	8	-7.23	7.14	5.53	133.79	35	33
	9	-3.88	-3.90	6.99	79.06	38	29
	10	0.16	-8.12	-2.91	74.32	34	29
	11	-2.12	-0.50	6.21	43.22	30	37
	12	13.99	-8.42	-0.90	267.25	32	33
	13	1.82	7.79	-5.64	95.88	31	32
	14	-8.61	-5.87	12.80	272.48	37	41
	15	8.80	3.29	7.75	148.40	34	36
	16	-15.00	-6.09	3.76	276.27	32	38
	17	4.75	-3.54	9.73	129.84	36	29
	18	-0.82	16.64	5.11	303.73	39	37
	19	4.48	9.18	-14.80	323.25	32	32
	20	-2.18	-11.00	5.76	159.01	35	29
	21	1.46	-8.70	6.77	123.61	27	31
	22	8.10	-11.03	-5.27	215.14	33	36
	23	17.37	3.31	-3.22	322.86	37	37
	24	3.76	-0.08	-7.90	76.63	33	34
	25	10.78	-2.44	-2.06	126.45	36	27
	26	8.49	4.78	4.49	114.99	40	38
	27	5.77	-1.22	-9.00	115.81	30	37
average		-0.07	-1.34	0.86	163.97	33	33
σ		8.44	7.19	6.68	110.08	3.51	3.86

Table 5.4: The investigation of the homogeneity of *neu_3*, a 'bad' structure.

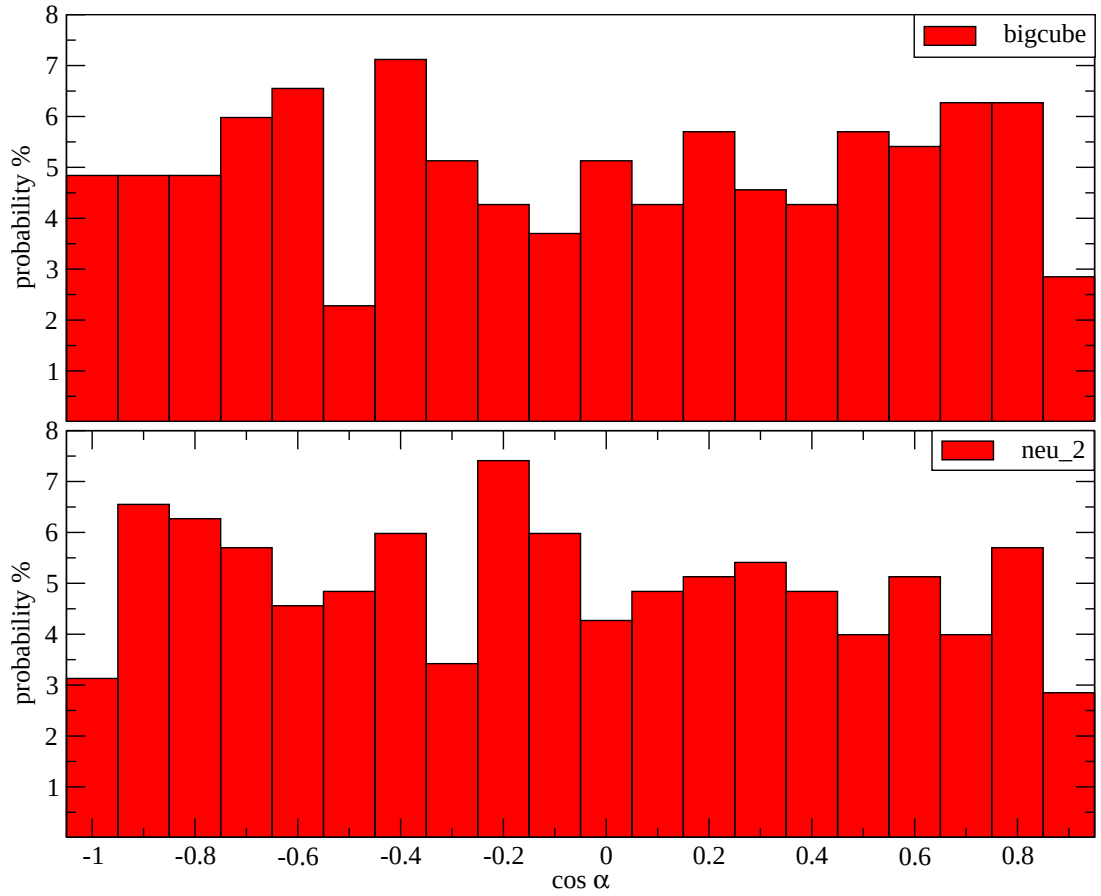

Figure 5.1: The histograms of the systems *bigcube* and *neu_2*. Both were 'good' relaxing structures. Plotted is the probability of the values of $\cos\alpha$.

5.2 Angular Distribution

As a next step, the angular distribution of the rotational dipole moment of the sub-boxes was calculated. This step seemed obvious, because it gives more information about the spatial arrangement than just the values of $\mathbf{M}_D^2$. This is due to the fact, that two different vectors can result in the same scalar. As an example serves Table 5.2, the vectors of box 3 and 7 of *neu_2* differ from each other but they have nearly the same scalar. Similar examples can be found for vectors of different systems too.

Therefore, the cosine α of the angle between two $\mathbf{M}_D$-vectors over all sub-boxes was computed:

$$\cos\alpha = \frac{\mathbf{M}_D^a \cdot \mathbf{M}_D^b}{|\mathbf{M}_D^a| \cdot |\mathbf{M}_D^b|}, \tag{5.1}$$

where a and b refer to the two vectors. The values were normalized and the results were printed out as probabilities in the histograms Fig. 5.1 and Fig. 5.2. The idea was that a 'bad' structure is more ordered than a 'good' structure. This means, for a 'bad' structure, that the cosine will

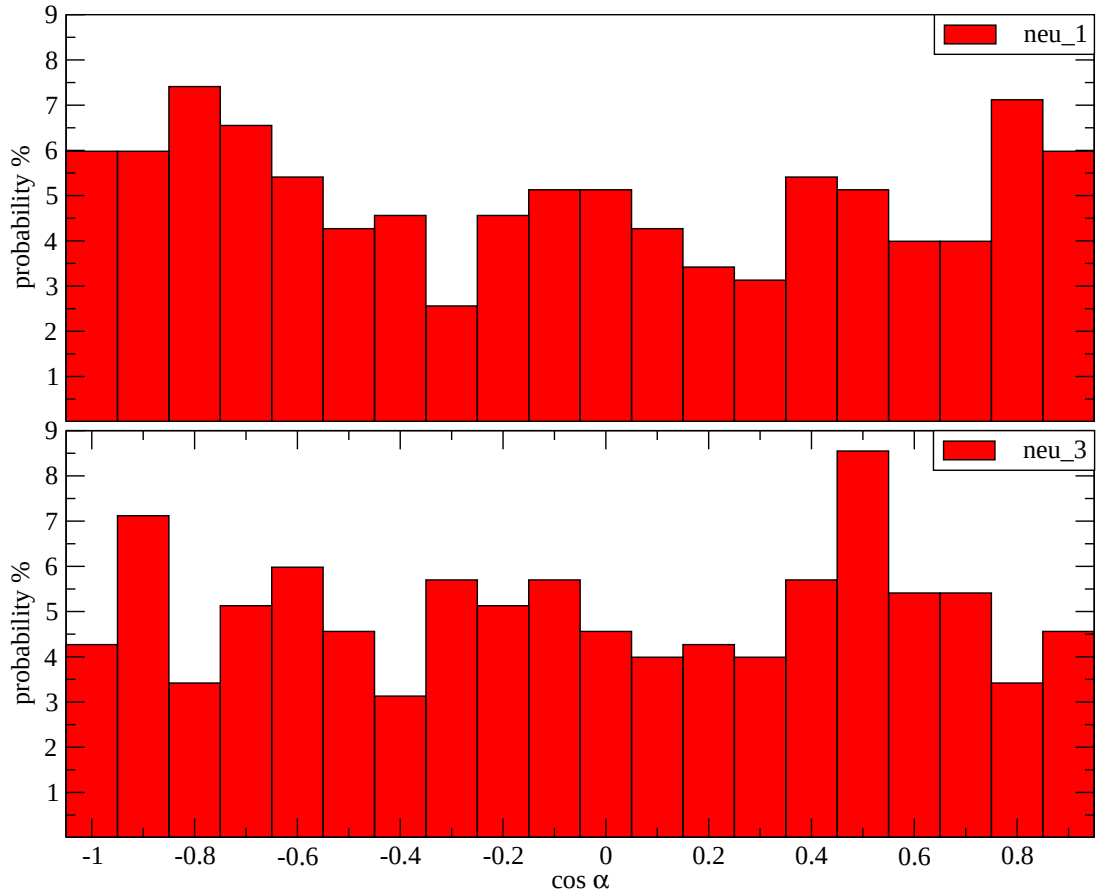

Figure 5.2: The histograms of the systems *neu_1* and *neu_3*. Both were 'bad' relaxing structures. Plotted is the probability of the values of $\cos\alpha$.

not range over the all possible values.

In Fig. 5.1 and Fig. 5.2 it is apparent, that the values for the cosine are well distributed. Again a trend could not be identified.

5.3 Spatial Composition assessed by Orientational Probability Functions

To gain a deeper insight in the spatial composition of these four systems, the orientational probability functions g^{000}_{++}, g^{000}_{--} and the mixed ones g^{000}_{+-} and g^{000}_{-+} were computed. The subscript $+$ refers to the cations and $-$ to the anions. Note, that these functions are identical with the radial distribution function. The g^{000} functions are plotted in Fig. 5.3 and Fig. 5.4. It is evident, that all the functions in each graph almost coincide. For the mixed functions one can see in Fig. 5.4, that they are identical, too. A difference for a 'good' or a 'bad' structure cannot be found in the radial packing.

Since the g^{000} functions do not differ from each other, it is the same for the charge ordering

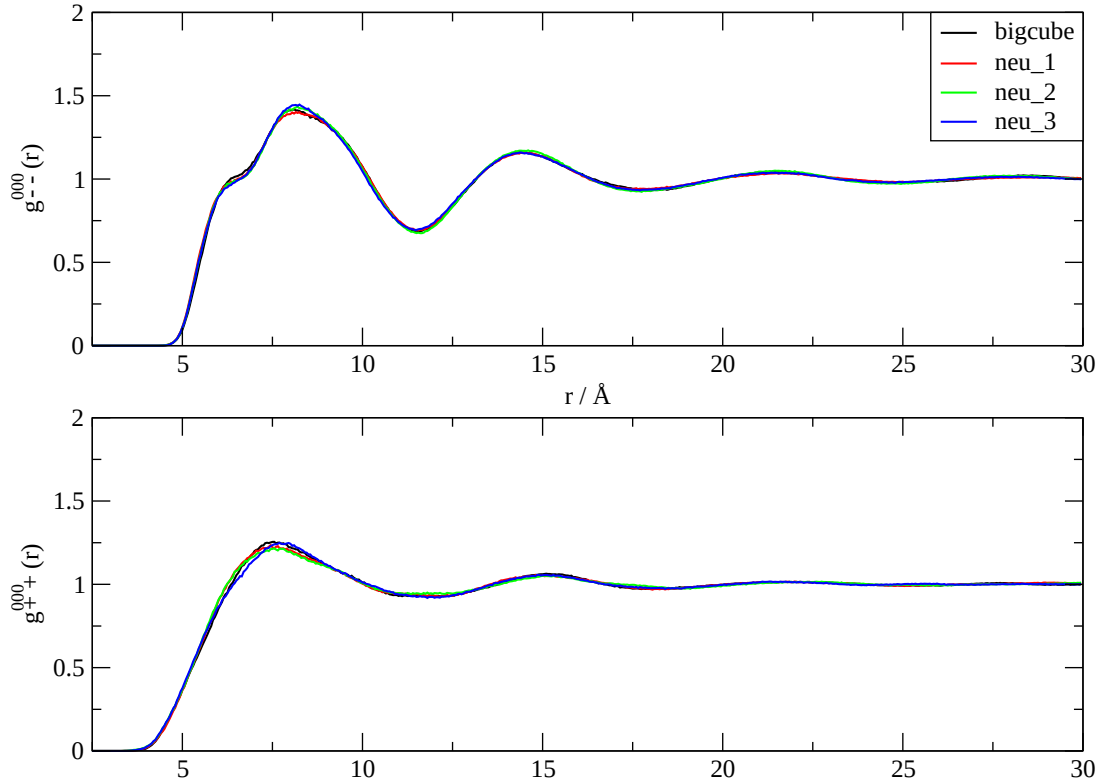

Figure 5.3: In the upper graph the anion was the reference point and the point of interest of the radial distribution function. The same goes for the cation in the lower graph. The functions in each graph are lying upon each other.

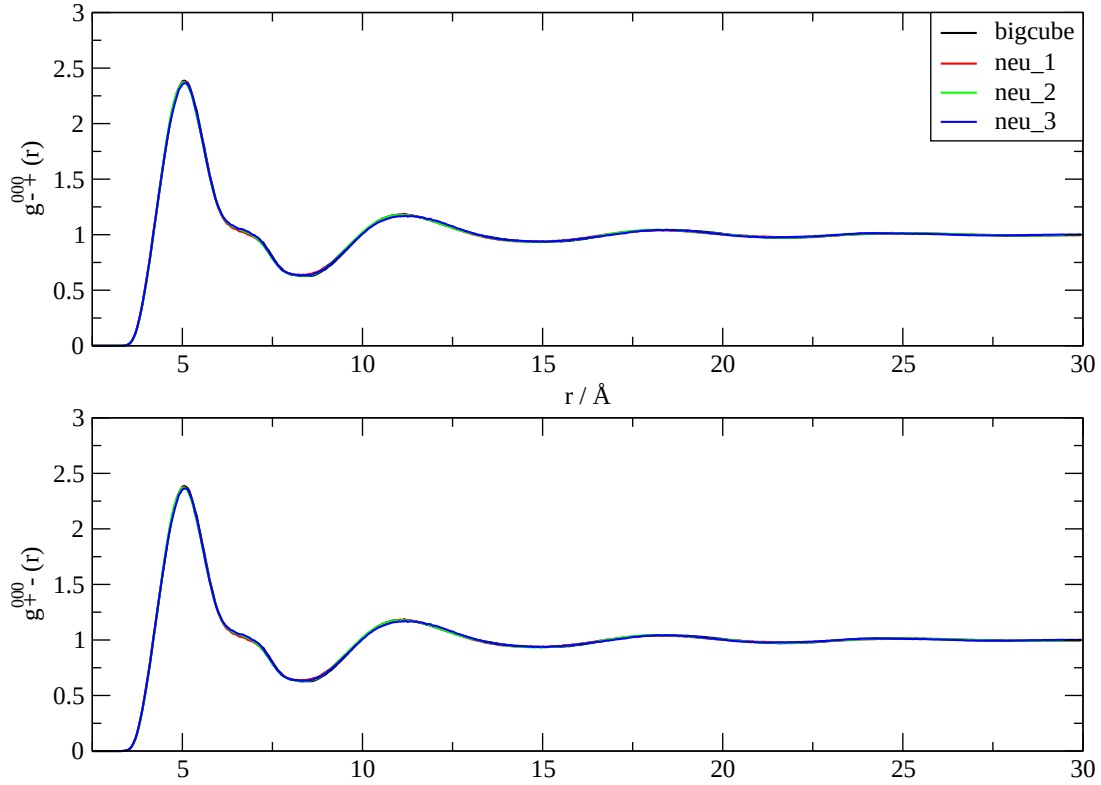

Figure 5.4: In the upper graph the anion was the reference point and the cation was the point of interest of the radial distribution function. For the lower graph it was the other way around. The functions in each graph are lying upon each other.

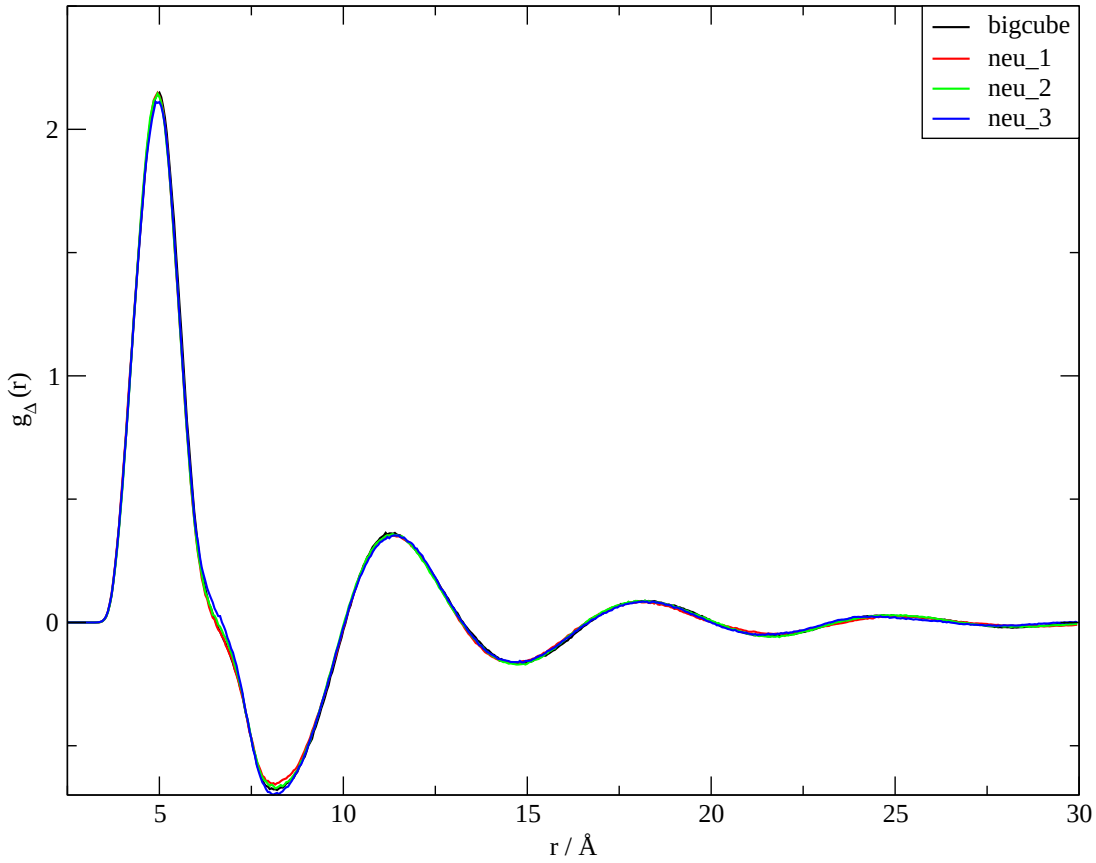

Figure 5.5: The charge ordering functions of the systems *bigcube* and *neu_1 - neu_3*.

functions of these systems. The charge ordering functions were computed according to Eqn. 3.29 and can be seen in Fig. 5.5.

Furthermore the functions g^{110}_{++}, g^{110}_{--}, g^{110}_{+-} and g^{110}_{-+}, which have a higher angular momentum were calculated by *GEPETTO*. The corresponing plots can be found in Fig. 5.6 and Fig. 5.7. The differences between the systems is due to the small values and is evident in the scaling of the y-axis and is therefore not of importance. A preferred direction for a 'good' or a 'bad' structure could not be identified. Again, it was not possible to distingiush between a 'good' and a 'bad' structure. In summary, the relaxation of systems cannot be observed in the orientational probability functions. The relaxation of the net rotational dipole moment $\mathbf{M}_D$ seems to be purely determined by collectivity and independent of short range or medium range structural ordering.

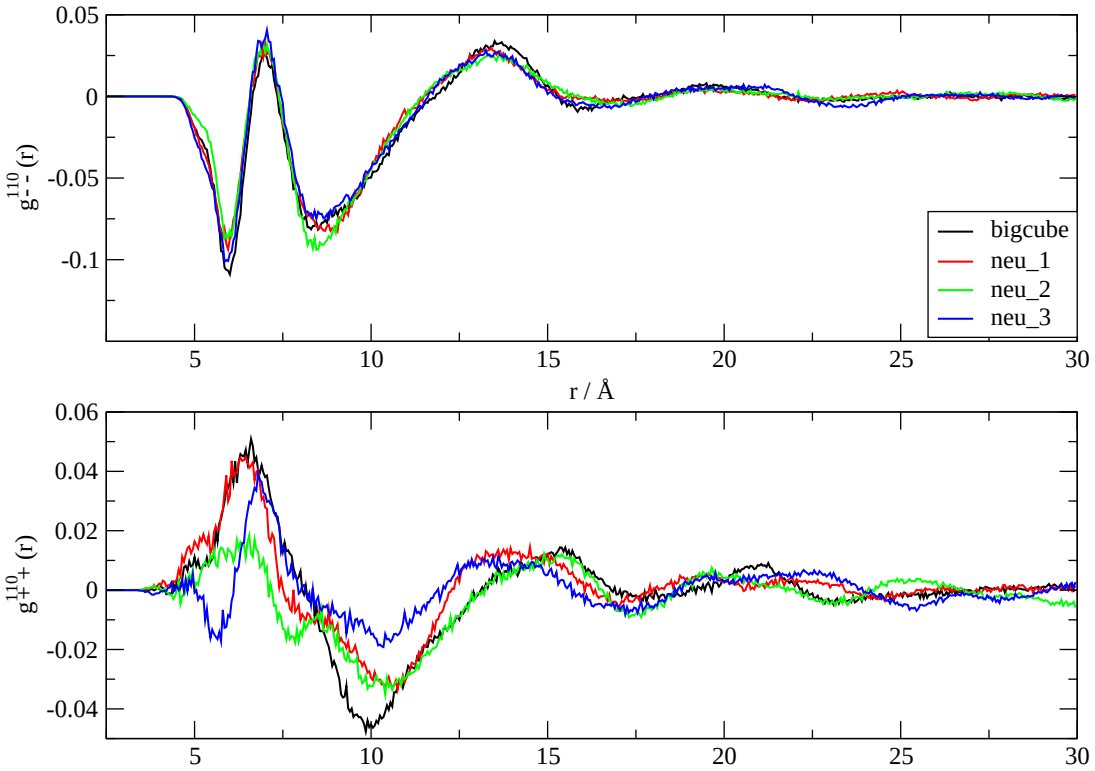

Figure 5.6: In the upper graph the anion was the reference point and the point of interest of the orientational probability function. The same goes for the cation in the lower graph. The functions in each graph are lying upon each other.

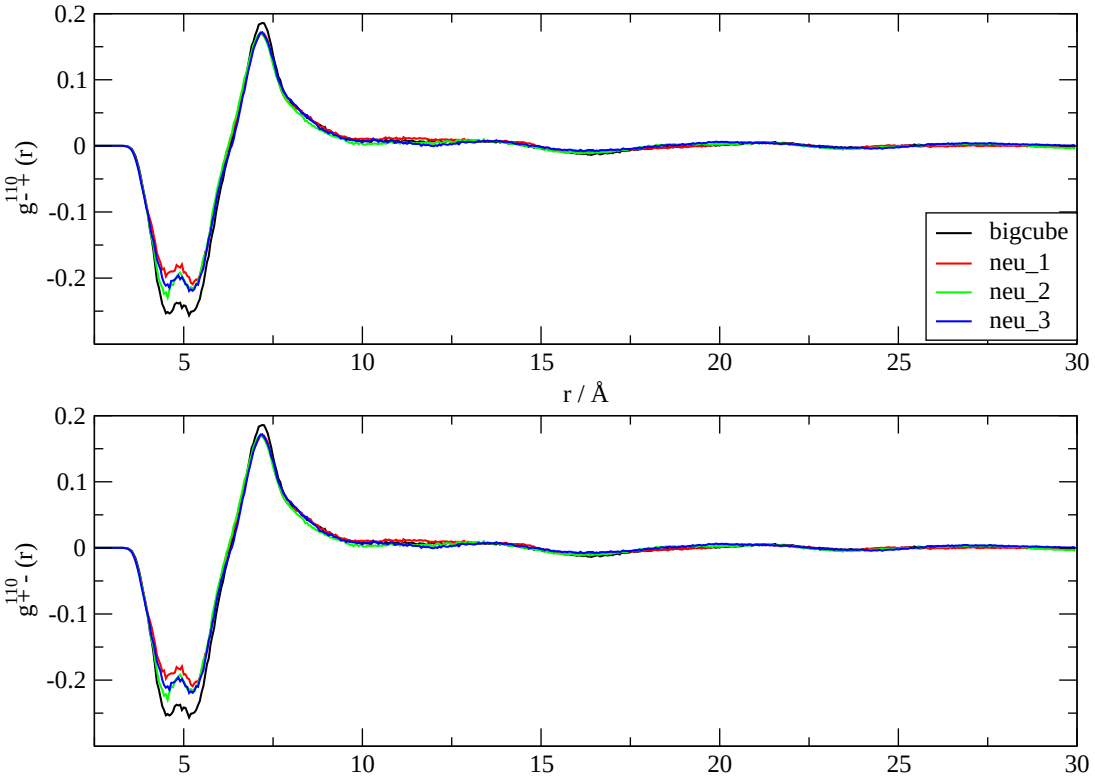

Figure 5.7: In the upper graph the anion was the reference point and the cation was the point of interest of the orientational probability function. For the lower graph it was the other way around. The functions in each graph are lying upon each other.

5.4 Separation of the Rotational Dipole Moment $\mathbf{M}_D$

The examination of the overall system did not deliver any insight why some structures relax, while others do not. Therefore, as another approach, the rotational dipole moment $\mathbf{M}_D$ was split up in the parts given by the cation $\mathbf{M}_D^+$ and the anion $\mathbf{M}_D^-$.

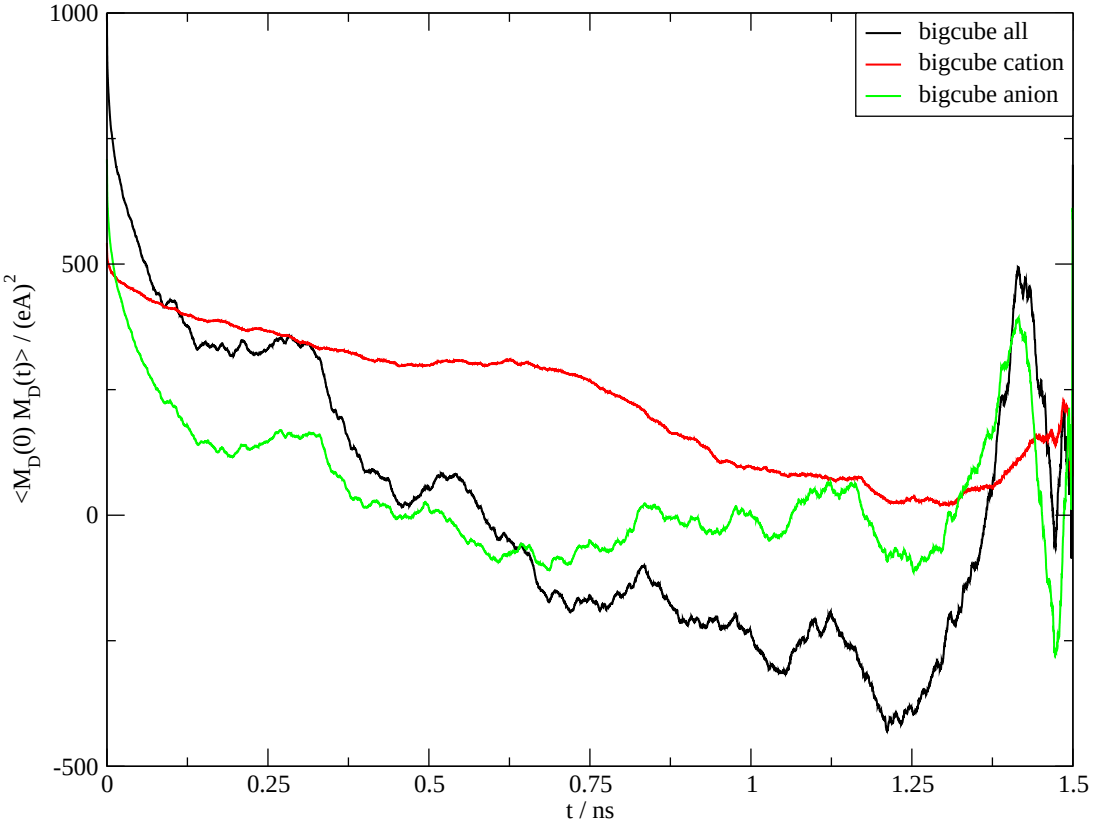

Figure 5.8: The correlation function for $\mathbf{M}_D$ of *bigcube*. The black curve gives the correlation function of the whole system, the red one is the contribution of the cation and the green one is of the anion.

The examination of the correlation functions gave an interesting result. For the structures *bigcube* and *neu_2*, which show a good relaxation, the contribution of the anion was greater than the contribution of the cation. For the systems *neu_1* and *neu_3*, the 'bad' relaxing structures, the values for the cation were a lot higher than those for the anion. For the exact values please examine Table 5.5.

Now, the correlation function $\langle \mathbf{M}_D(0) \cdot \mathbf{M}_D(t) \rangle$ of the systems bigcube, neu_1 up to neu_4 and 69_1 up to 69_4 were fitted multiexponential according to:

$$\langle \mathbf{M}_D(0) \cdot \mathbf{M}_D(t) \rangle = \sum_i A_i \cdot e^{-t/\tau_i}. \tag{5.2}$$

Most of the correlation functions were fitted tri-exponentially, except of *neu_4* and *69_1*, which

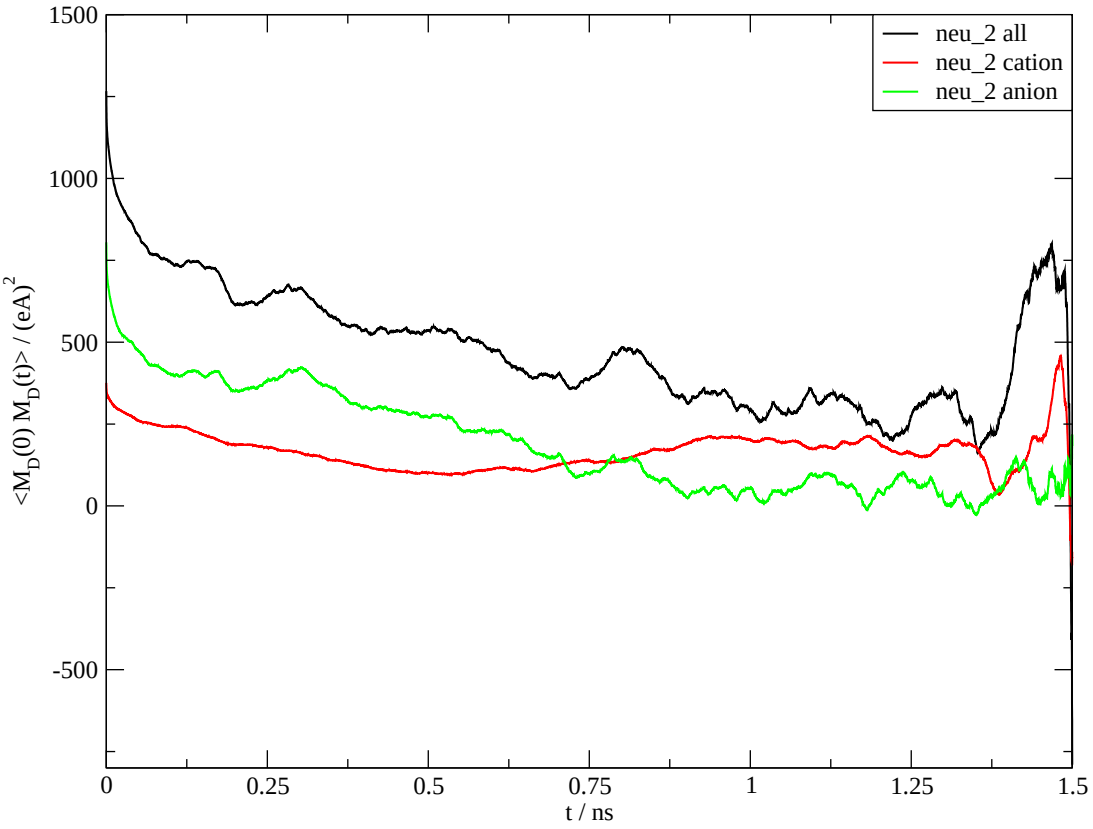

Figure 5.9: The correlation function for $\mathbf{M}_D$ of *neu_2*. The black curve gives the correlation function of the whole system, the red one is the contribution of the cation and the green one is of the anion.

Name	$(\mathbf{M}_D)^2$ all	$(\mathbf{M}_D^+)^2$ cation	$(\mathbf{M}_D^-)^2$ anion
bigcube	999.2	542.1	708.6
neu_2	1266.6	375.8	804.8
neu_1	3502.9	2489.1	634.8
neu_3	3397.6	1435.7	983.1

Table 5.5: The starting values of the correlation functions with the values of the contribution of the cation and the anion. For structures, which relax well, the contribution of the anion is higher than the contribution of the cation.

needed only two exponentials. The functions were fitted over a time period of 1.5 nanoseconds.

The corresponing fit parameters are tabulated in Table 5.6.

For the characterization of these correlation functions the tabulated parameters were subsumed to an average relaxation time constant $< \tau >$ computed by

$$< \tau >= \frac{\sum_i A_i \cdot \tau_i}{\sum_i A_i}. \tag{5.3}$$

Please, note that these parameters A_i and τ_i are gained from the total collective rotational dipole moment $\mathbf{M}_D$.

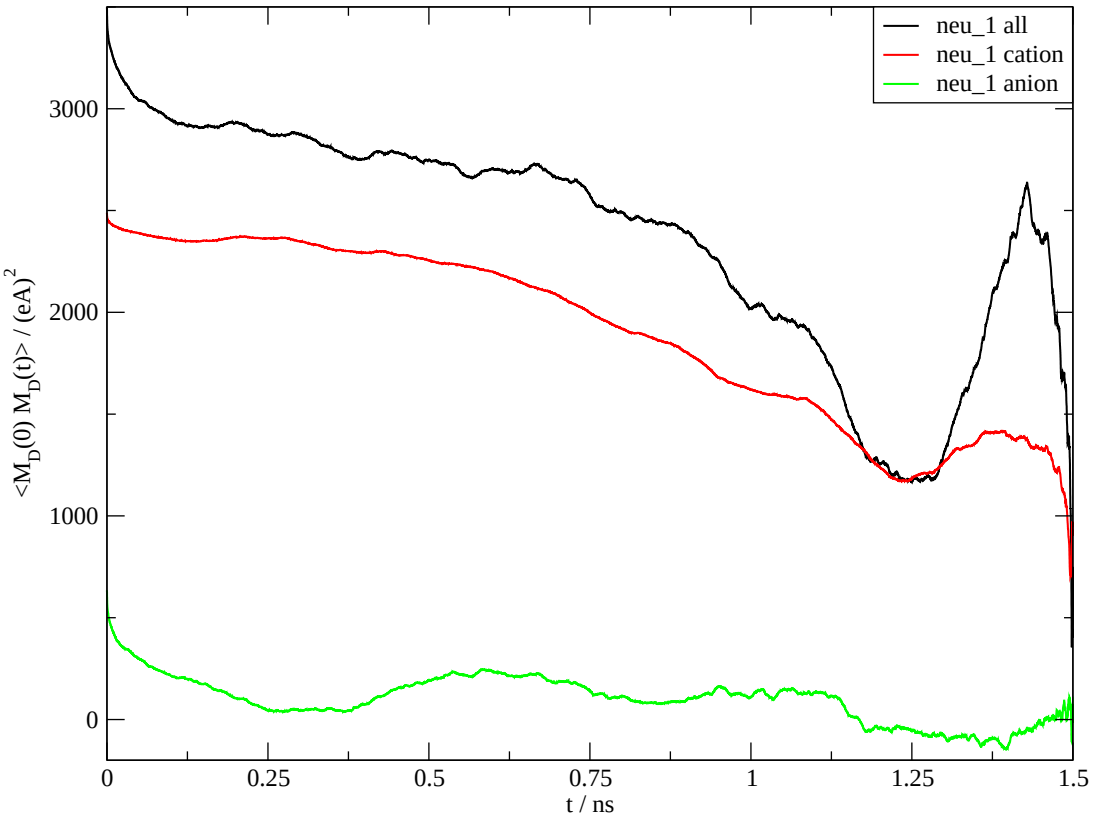

Figure 5.10: The correlation function for $\mathbf{M}_D$ of *neu_1*. The black curve gives the correlation function of the whole system, the red one is the contribution of the cation and the green one is of the anion.

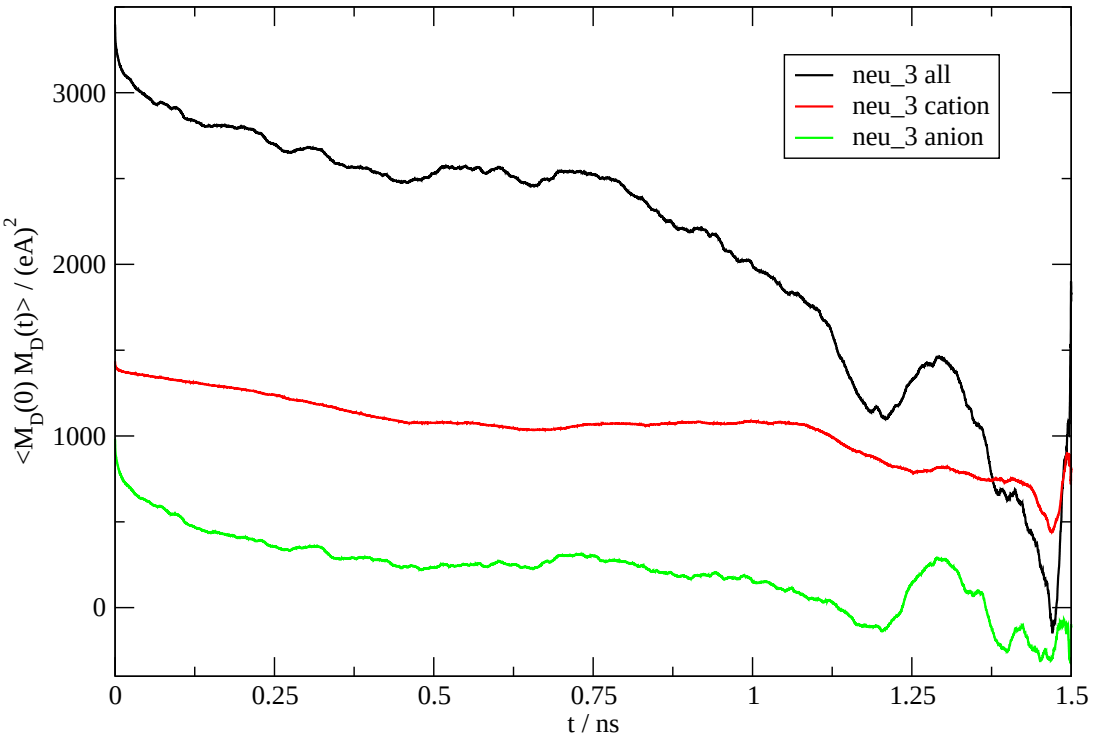

Figure 5.11: The correlation function for $\mathbf{M}_D$ of *neu_3*. The black curve gives the correlation function of the whole system, the red one is the contribution of the cation and the green one is of the anion.

Name	A_1	τ_1	A_2	τ_2	A_3	τ_3	$<\tau>$	$(\mathbf{M}_D)^2$ all	$(\mathbf{M}_D^+)^2$ cation	$(\mathbf{M}_D^-)^2$ anion
	$(eA)^2$	ps	$(eA)^2$	ps	$(eA)^2$	ps	ps	$(eA)^2$	$(eA)^2$	$(eA)^2$
bigcube	66.9	0.2	175.8	3.3	764.1	194.0	147.8	999.2	542.1	708.6
neu_4			222.2	10.9	1713.5	653.0	579.3	2024.0	1386.2	604.5
69_1			180.8	3.9	1786.6	653.0	593.3	2024.0	966.8	662.7
69_2	46.6	0.4	142.0	3.2	2846.0	848.0	795.5	2790.9	1374.8	663.4
69_3	146.2	2.3	520.7	75.4	531.7	1856.1	856.4	1241.3	462.1	612.2
neu_2	273.1	14.4	280.3	228.0	609.9	2000.0	1106.8	1266.6	375.8	804.9
neu_3	105.7	1.0	175.8	10.5	3093.8	1516.0	1390.2	3397.6	1435.7	983.1
69_4	86.1	0.2	250.1	9.0	2976.3	1659.0	1491.3	3303.1	1499.4	711.8
neu_1	128.8	0.4	288.1	18.4	3096.9	2260.0	1993.4	3502.9	2489.1	634.9

Table 5.6: The fit parameters of the BMIM_TRIF_891-systems. The systems are ordered according to the increasing values ot the average τ, $<\tau>$.

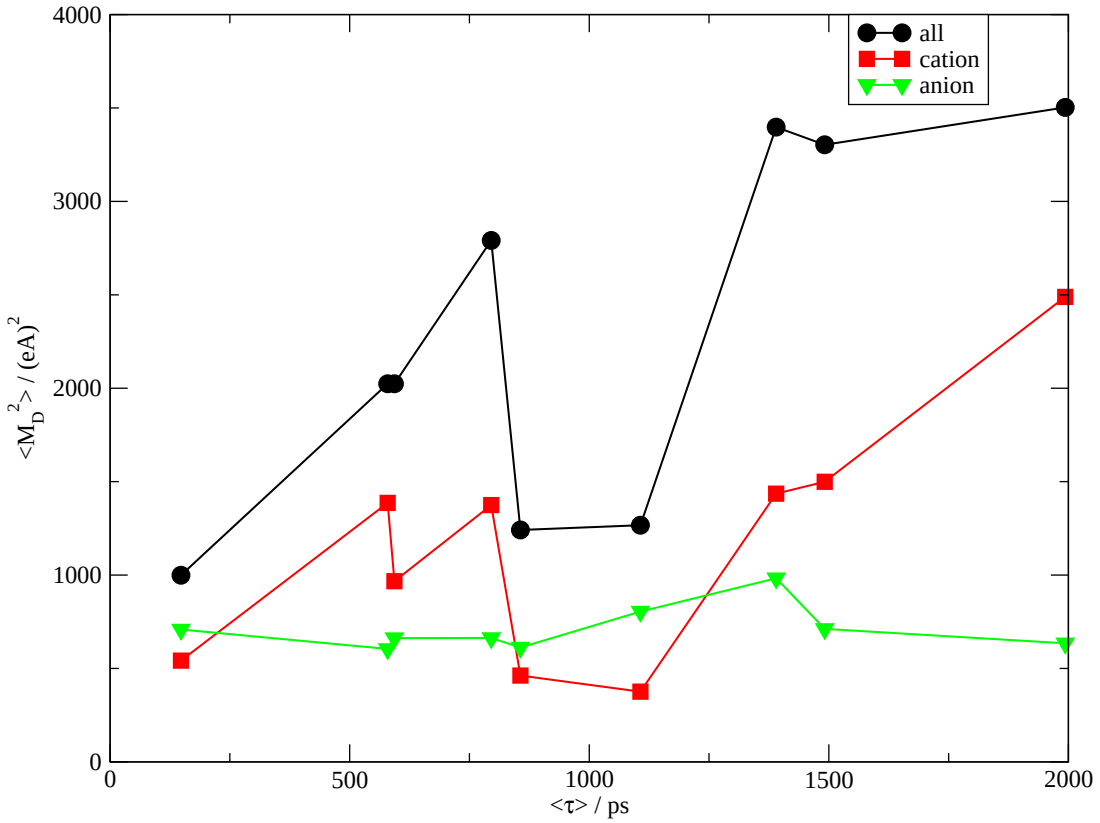

Figure 5.12: The average time $< \tau >$ of the systems *bigcube*, *neu_1* - *neu_4* and *69_1* - *69_4* plotted against $(\mathbf{M}_D)^2$, $(\mathbf{M}_D^+)^2$ and $(\mathbf{M}_D^-)^2$.

In Fig. 5.12 $< \tau >$ was plotted versus $\mathbf{M}_D^2$ and its contributions from the cations $(\mathbf{M}_D^+)^2$ and anions $(\mathbf{M}_D^-)^2$.

The total $\mathbf{M}_D^2$ seems to increase roughly linear with increasing $< \tau >$ indicating a Kivelson-Madden relationship [32, 33].

In principle, $\mathbf{M}_D$ can be decomposed into its cationic $\mathbf{M}_D^+$ and anionic $\mathbf{M}_D^-$ contributions. Consequently, $\mathbf{M}_D^2$ contains pure cationic and pure anionic as well as mixed contributions. The latter one were neglected in the present study.

The rise of $\mathbf{M}_D^2$ in Fig. 5.12 seems to be mainly due to the BMIM contribution, which also shows the trend as visible by the red line in Fig. 5.12. In contrast, the Triflate based $\mathbf{M}_D^-$ is almost unaffected by $< \tau >$ as visible by the green line in Fig. 5.12.

One may conclude that the relaxation of the anions is much faster than that of the cations, which are responsible for the very large values of $< \tau >$. In other words, the shorter time constants τ_1 and τ_2 in Table 5.6 are affected by the anions. In contrast, the last time constant τ_3 dominating the calculation of $< \tau >$ characterizes the rotational relaxation of the cations.

6 EMIM_TRIF_891

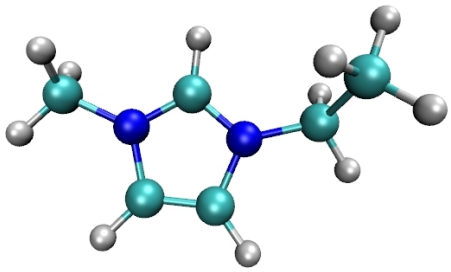

Figure 6.1: The cation 1-Ethyl-3-methyl-imidazolium (EMIM)

To gain a deeper insight a different system was set up. This time 1-Ethyl-3-methyl-imidazolium (EMIM) served as the cation, the anion stayed the same. EMIM (Fig. 6.1) is a smaller molecule than BMIM and has a smaller dipole moment, too. Again 891 ion pairs were packed according to the experimental density into a box (Table 6.1). Due to the fact, that EMIM requires less space than BMIM, the box had only an edge length of 65.3Å.

Name	seed
emim_1	187
emim_2	385
emim_3	692
emim_4	471
emim_5	297
emim_6	803
emim_7	546
emim_8	773
emim_9	920
emim_10	143

Table 6.1: The EMIM_TRIF_891-systems packed by PACKMOL.

As already done for the BMIM_TRIF_891-systems, the correlation functions $\langle \mathbf{M}_D(0) \cdot \mathbf{M}_D(t) \rangle$ of these systems were split up in a cationic $\mathbf{M}_D^+$ and an anionic $\mathbf{M}_D^-$ contribution. The replacement of the cation BMIM by EMIM had a great influence on the relaxation of the total system. Now, the relaxation was mostly dependent on the anion instead of the cation. As an example of a 'good' relaxing structure serves *emim_2* (Fig. 6.2). One can see in Fig. 6.2, that the cation (red

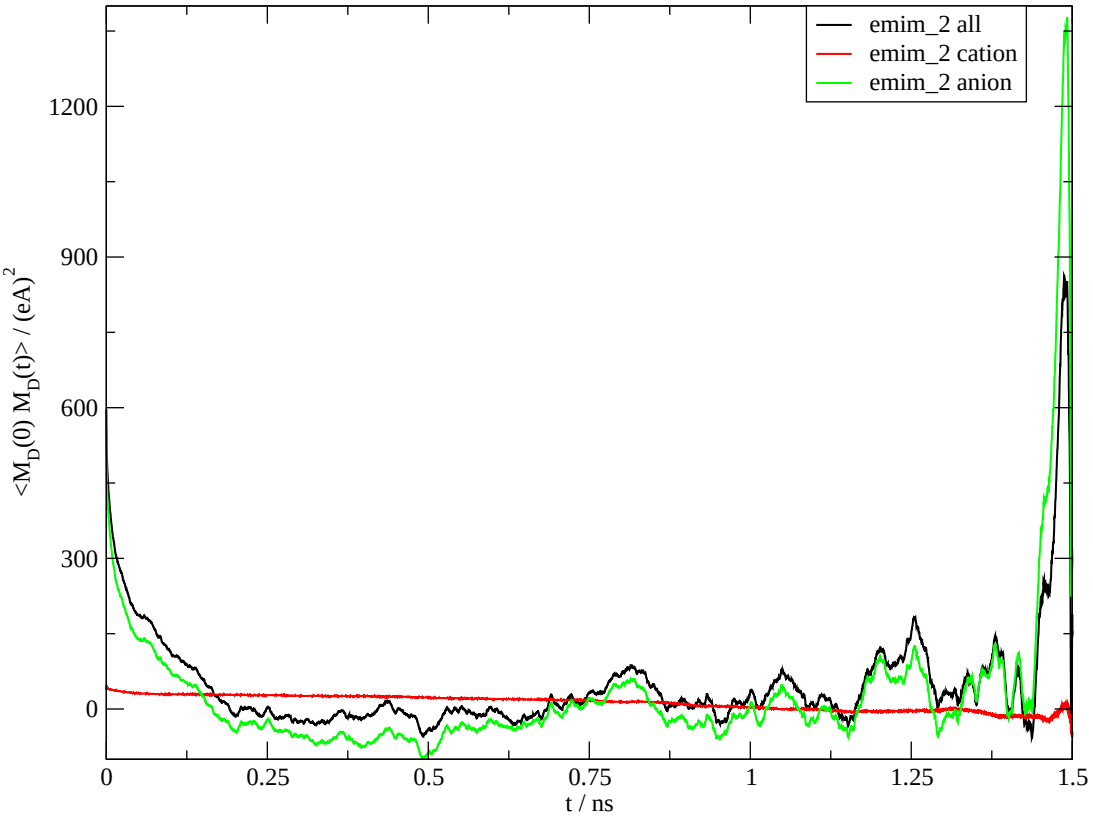

Figure 6.2: The correlation function for $\mathbf{M}_D$ of *emim_2*. The black curve gives the correlation function of the whole system, the red one is the contribution of the cation and the green one is of the anion. *emim_2* is an example for a 'good' structure.

line) does not contribute much to the total correlation function, but even that small part does not decline either. In Fig. 6.3 there is an example for a 'bad' structure. Although the anion (green line) relaxes fast, the contribution of the cation is quite high. The fact, that the cation does not relax, keeps the correlation function from declining to zero.

The correlation functions of all EMIM_TRIF_891-systems were fitted multiexponential over a time period of 1.5 nanoseconds. For the systems *emim_1*, *emim_2*, *emim_4*, *emim_7* and *emim_9* a bi-exponential fit was sufficient. For the systems *emim_3*, *emim_5*, *emim_6* and *emim_9* three exponentials were needed. For the exact fit parameters of the systems examine Table 6.2. The system *emim_10* could not be fitted satisfactorily and does not appear in Table 6.2 or in Fig. 6.4.

The average relaxation time $< \tau >$ was plotted versus $\mathbf{M}_D^2$ and its contributions from the cations $(\mathbf{M}_D^+)^2$ and anions $(\mathbf{M}_D^-)^2$, which can be seen in Fig. 6.4. Again a Kivelson-Madden relationship [32,33] could be identified, due to the fact, that $\mathbf{M}_D^2$ increases together with $< \tau >$. In contrast to the BMIM_TRIF_891-systems, the relaxation of $\mathbf{M}_D^2$ is mainly due to the anionic contribution. Although, the short time constant $< \tau_1 >$ in Table 6.2 is affected by the anions. The longer time constants $< \tau_2 >$ and $< \tau_3 >$ belong to the cations.

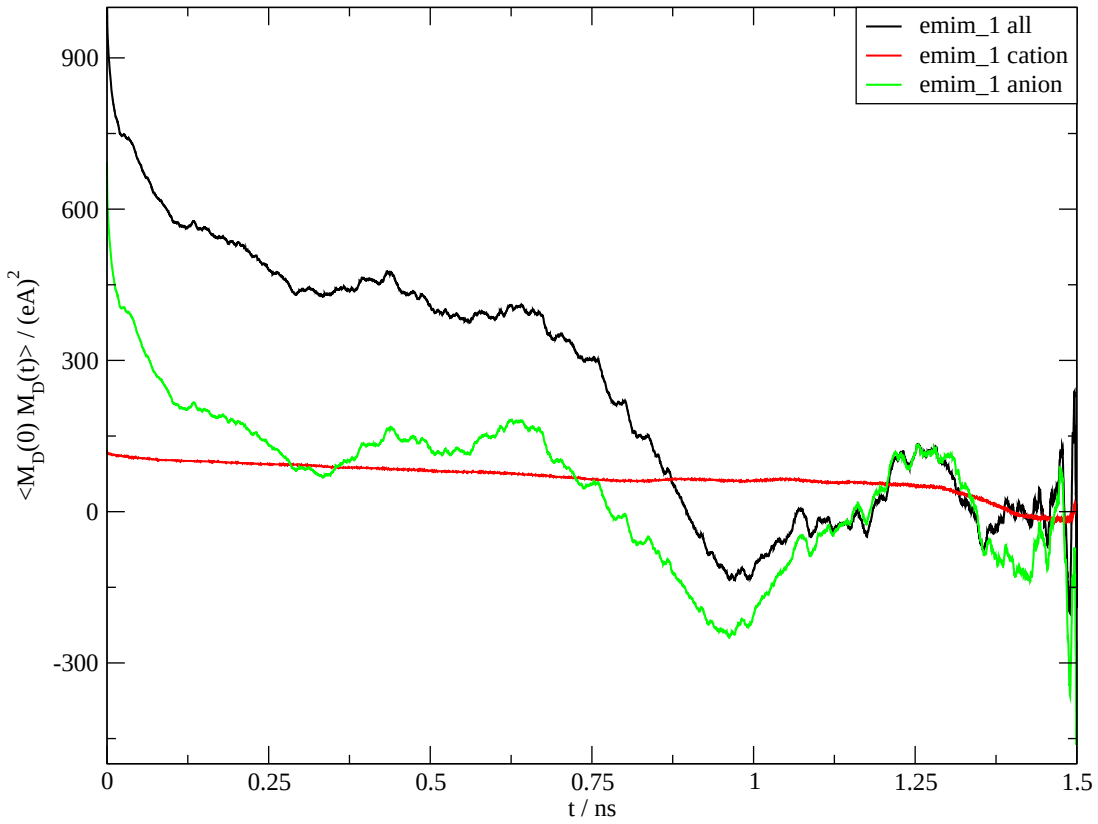

Figure 6.3: The correlation function for $\mathbf{M}_D$ of *emim_1*. The black curve gives the correlation function of the whole system, the red one is the contribution of the cation and the green one is of the anion. *emim_1* is an example for a 'bad' structure.

In Fig. 6.4 the red line resembles the cations and does not give much contribution to the total $\mathbf{M}_D^2$. The anionic contribution is visible in the green line in Fig. 6.4 and one can see, that the anions give the trend $\mathbf{M}_D^2$.

Name	A_1	τ_1	A_2	τ_2	A_3	τ_3	$<\tau>$	$(\mathbf{M}_D)^2$ all	$(\mathbf{M}_D^+)^2$ cation	$(\mathbf{M}_D^-)^2$ anion
	$(eA)^2$	ps	$(eA)^2$	ps	$(eA)^2$	ps	ps	$(eA)^2$	$(eA)^2$	$(eA)^2$
emim_2	168.2	3.2	392.1	71.0			50.6	596.9	48.4	538.4
emim_8	118.6	1.4	372.6	58.3	127.6	264.8	90.0	643.8	83.9	554.4
emim_3	128.9	2.0	277.0	44.0	226.0	226.6	100.8	665.0	102.8	614.4
emim_4	164.8	4.8	646.6	158.7			127.5	864.3	66.9	742.5
emim_7	190.7	0.9	884.0	190.6			157.0	1026.3	87.9	817.5
emim_9	220.9	6.3	477.5	311.6			215.0	748.8	106.9	595.2
emim_5	177.5	6.0	426.8	107.2	92.2	1250.0	232.7	756.3	71.7	804.3
emim_6	284.2	19.2	221.1	131.2	339.8	701.9	323.0	936.4	118.6	674.4
emim_1	198.0	3.8	808.8	515.5			414.9	1041.4	122.5	693.2

Table 6.2: The fit parameters of the EMIM_TRIF_891-systems. The systems are ordered according to the increasing values ot the average τ, $<\tau>$.

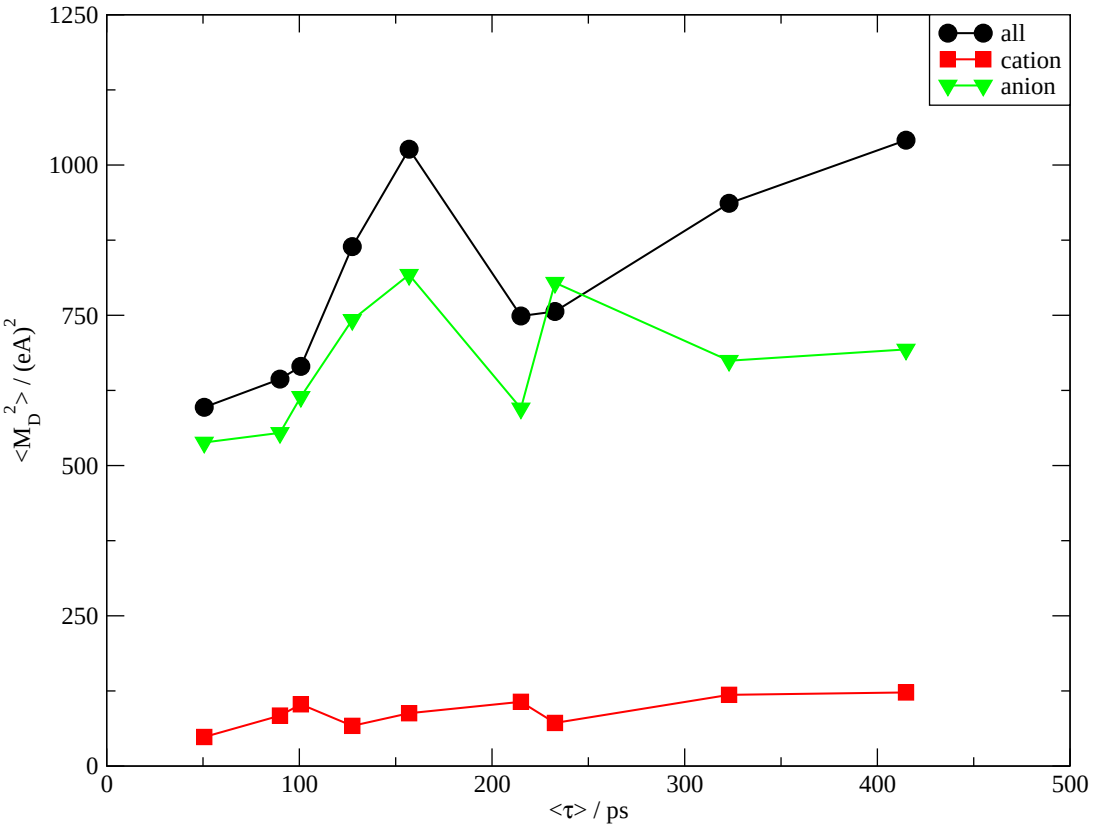

Figure 6.4: The average time $< \tau >$ of the systems *emim_1* - *emim_9* plotted against $(\mathbf{M}_D)^2$, $(\mathbf{M}_D^+)^2$ and $(\mathbf{M}_D^-)^2$.

7 Conclusion

This thesis had two main points. First, the generation of new start configurations, which can be used for molecular dynamics simulation and second, the assessment of these newly created systems.

For the generation of new starting configurations, PACKMOL [13] is the method of choice. It is possible to pack any number of different molecules, also ions, into a box of defined size. Furthermore, the molecules in the boxes are well distributed and only a minimization of the energy is necessary, before one is able to start the simulation. The option *seed* [13] provides the user with the possibility to pack the same number of molecules in a box of the same size, but with a different spatial composition.

In addition, the program convinces with its short computation time, from a few seconds up to a few minutes.

In this thesis two different ionic liquids were examined. The ionic liquid BMIM_TRIF_891 consisted of the cation 1-Butyl-3-methyl-imidazolium and the anion Triflate, while the other ionic liquid EMIM_TRIF_891 had as a cation 1-Ethyl-3-methyl-imidazolium, the anion stayed the same.

After packing the molecules into a box and a minimization of the energy, one is able to start the simulation. All simulations were carried out by the molecular dynamics program CHARMM [14]. Note, that an adjustment of the coordinate systems is needed before one is able to start a simulation in CHARMM. After simulating the same structures with different velocities, I found out, that the relaxation of starting structures is dependent of their spatial composition and not of the assigned velocity at the beginning of a simulation. This effect can be seen in Fig. 4.16 and Fig. 4.17.

The assessment, if a structure is relaxed or not, was done by correlation functions [23] of the total rotational moment, $\langle \mathbf{M}_D(0) \cdot \mathbf{M}_D(t) \rangle$. Note, that $\mathbf{M}_D$ is a collective property.

As a next step, the spatial composition of start configurations was investigated. The orientational probability functions [22, 24–26] give an insight in the short and medium range order. But a reason for the relaxation of some structures, while others do not, could not be identified. This

is evident in Fig. 5.3, 5.4, 5.6 and 5.7. Therefore, the relaxation of molecular ions has to be an effect of the collectivity.

Only the decomposition of the rotational moment $\mathbf{M}_D$ into the cationic $\mathbf{M}_D^+$ and the anionic $\mathbf{M}_D^-$ contribution gave a deeper insight, why some structures relax, while others do not. Cross terms were neglected in this study.

For the BMIM_TRIF_891-systems the relaxation was dependent on the cation, which had the greatest contribution to the total rotational moment $\mathbf{M}_D$. In Fig. 5.10 one can see, that the rapid relaxation at the beginning is mostly affected by the anions and the following slower decline is a result of the cations. This is due to the fact, that the cation BMIM has the greatest molecular dipole moment of the three investigated ions and it rotates the slowest. The anion does not contribute much to the total rotational moment $\mathbf{M}_D^2$.

Furthermore, the correlation functions $\left\langle \mathbf{M}_D(0) \cdot \mathbf{M}_D(t) \right\rangle$ of these systems were fitted multiexponentially. The longer relaxation times in Table 5.6 belong to the cation BMIM and this again is an indication for their slow rotation and therefore, relaxation. The short relaxation times belong to the anions.

An average relaxation time $< \tau >$ was computed too. The average relaxation time $< \tau >$ was plotted versus $\mathbf{M}_D^2$ and its contributions from the cations $(\mathbf{M}_D^+)^2$ and anions $(\mathbf{M}_D^-)^2$. One can see in Fig. 5.12, that the red line gives the trend in the rise of $\mathbf{M}_D^2$ (black line).

The fact, that $< \tau >$ increased with increasing $\mathbf{M}_D^2$, indicated a Kivelson-Madden relationship [32, 33].

For the EMIM_TRIF_891-systems, it was a bit different. The examination of Fig. 6.3 showed, that the fast relaxation at the beginning is again only affected by the anions. The fact, that EMIM has the smallest dipole moment compared to BMIM and TRIF, results in a smaller contribution to the total $\mathbf{M}_D^2$. Nevertheless, EMIM rotates quite slow, which can be seen in the red line in Fig. 6.3. The cationic contribution of the correlation function does not decline much, but it must not be neglected.

The correlation functions of the EMIM_TRIF_891-systems were fitted too and the relaxation times τ_i are tabulated in Table 6.2. Again the short relaxation times belong to the anion TRIF and the long ones to the cation EMIM.

The average relaxation time $< \tau >$ was plotted versus $\mathbf{M}_D^2$, $(\mathbf{M}_D^+)^2$ and $(\mathbf{M}_D^-)^2$ and this time the anion (green line) was responsible for the trend $\mathbf{M}_D^2$. A Kivelson-Madden relationship [32, 33] could be identified for these systems, too.

One may conclude, that the decomposition of the rotational moment $\mathbf{M}_D^2$ gives an indication

about the extent of the contribution of the cations $(\mathbf{M}_D^+)^2$ and anions $(\mathbf{M}_D^-)^2$, but only for one system at the time. The relaxation time of the cations is in general greater, because they are bigger and more anisotropic than the anions. Is the contribution $(\mathbf{M}_D^+)^2$ of the cations a lot bigger than the anionic contribution $(\mathbf{M}_D^-)^2$, the structure is probably 'bad'. For the case, that the cationic contribution is smaller than the anionic, the resulting structure may show a good relaxation behaviour.

In addition, the multiexponential fit of the correlation function $\langle \mathbf{M}_D(0) \cdot \mathbf{M}_D(t) \rangle$ provides relaxation times τ_i for the cations and anions. The relaxation times give information about how fast molecules rotate and therefore, are able to relax. A long relaxation time means a slow relaxation manner and vice versa.

The average relaxation time $< \tau >$ plotted versus $\mathbf{M}_D^2$, $(\mathbf{M}_D^+)^2$ and $(\mathbf{M}_D^-)^2$ tells us, which ion species contributes the most to the total correlation function $\langle \mathbf{M}_D(0) \cdot \mathbf{M}_D(t) \rangle$.

Bibliography

[1] Z.-B. Zhou, H. Matsumoto, K. Tatsumi: Chem. Phys. Chem., **6**, 1324 (2005).

[2] M. Freemantle, C. London: Science & Technology, **82**, 44 (2004).

[3] E. Amigues, C. Hardacre, G. Keane, M. Migaud, M. O'Neill: Chem. Commun., 72 (2006).

[4] D. W. Rooney, K. R. Seddon: *Handbook of solvents*, ChemTec, Toronto (2001).

[5] A. Kawai, T. Hidemori, K. Shibuya: Chem. Letters, **33**, 1464 (2004).

[6] C. Wakai, A. Oleinikova, M. Ott, H. Weingärtner: J. Phys. Chem. B, **109**, 17028 (2005).

[7] G.-H. Tao, M. Z. und Xiao-Hua Wang, Z. yu Chen, D. G. Evans, Y. Kou: Aust. J. Chem., **58**, 327 (2005).

[8] R. Hagiwara, Y. Ito: J. Fluorine Chem., **105**, 221 (2000).

[9] T. Welton: Chem. Rev., **99**, 2071 (1999).

[10] S. T. Handy, X. Zhang: Org. Lett., **3**, 233 (2001).

[11] C. M. Gordon: App. Cat. A, **222**, 101 (2001).

[12] A. E. Visser, R. P. Swatloski, W. M. Reichert, J. H. Davis, Jr, R. D. Rogers: Chem. Commun., **1**, 135 (2001).

[13] L. Martínez, R. Andrade, E. Birgin, J. Martínez: J. Comp. Chem., **0**, 0 (2009).

[14] B. R. Brooks, C. L. B. III, A. D. M. Jr., L. Nilsson, R. J. Petrella, B. Roux, Y. Won, G. Archontis, C. Bartels, S. Boresch, A. Caflisch, L. Caves, Q. Cui, A. R. Dinner, M. Feig, S. Fischer, J. Gao, M. Hodoscek, W. Im, K. Kuczera, T. Lazaridis, J. Ma, V. Ovchinnikov, E. Paci, R. W. Pastor, C. B. Post, J. Z. Pu, M. Schaefer, B. Tidor, R. M. Venable, H. L. Woodcock, X. Wu, W. Yang, D. M. York, M. Karplus: J. Comput. Chem., **30**, 1545 (2009).

[15] Http://www.charmm.org/documentation/c35b1/minimiz.html.

[16] Http://www.charmm.org/documentation/c35b1/pressure.html.

[17] Http://www.charmm.org/documentation/c35b1/nose.html.

[18] Http://www.charmm.org/documentation/c35b1/scalar.html.

[19] C. Schröder, O. Steinhauser: J. Grunenberg, ed., *Computational Spectrometry*, Wiley-VCH, Weinheim (2010).

[20] C. Schröder, O. Steinhauser: J. Chem. Phys., **131**, 114504 (2009).

[21] C. Schröder, M. Haberler, O. Steinhauser: J. Chem. Phys., **128**, 134501 (2008).

[22] C. Schröder, T. Rudas, G. Neumayr, W. Gansterer, O. Steinhauser: J. Chem. Phys., **127**, 044505 (2007).

[23] J. P. Hansen, I. R. McDonald: *Theory of Simple Liquids*, 2nd edition, Pergamon, New York (1986).

[24] C. Schröder, T. Rudas, O. Steinhauser: J. Chem. Phys., **125**, 244506 (2006).

[25] P. Höchtl, S. Boresch, W. Bitomsky, O. Steinhauser: J. Chem. Phys., **109**, 4927 (1998).

[26] O. Steinhauser: Ber. Bunsenges. Phys. Chem., **87**, 128 (1983).

[27] M. Neumann, O. Steinhauser: Chem. Phys. Lett., **102**, 508 (1983).

[28] O. Steinhauser, H. Bertagnolli: Ber. Bunsenges. Phys. Chem., **85**, 45 (1981).

[29] L. Blum, A. H. Narten: Adv. Chem. Phys., **34**, 203 (1976).

[30] A. J. Stone: Mol. Phys., **36**, 241 (1978).

[31] Http://www.charmm.org/documentation/c35b1/ewald.html.

[32] P. Madden, D. Kivelson: Mol. Phys., **30**, 1749 (1975).

[33] P. Madden, D. Kivelson: Adv. Chem. Phys., **56**, 467 (1984).

CURRICULUM VITAE

Sonja Maurer

Wien, 20.03.2010

25.07.1985	geboren in Mödling
1991 - 1995	Volksschule 2, Dr. Karl Renner Straße, Guntramsdorf
1995 - 2003	BG/BRG Baden Frauengasse
Juni 2003	Matura mit gutem Erfolg
WS 2003/04	Diplomstudium Medizin an der Universität Wien
seit SS 2004	Diplomstudium Chemie an der Universität Wien
WS 2007/08	Erasmusstipendium für University of Warwick, Coventry (GB)
seit Februar 2009	Diplomarbeit bei Prof. O. Steinhauser am Institut für Computergestützte biologische Chemie